PAUL SCHERRER INSTITUT

PSI

SwissFEL
Injector Conceptual Design Report

Accelerator test facility for SwissFEL

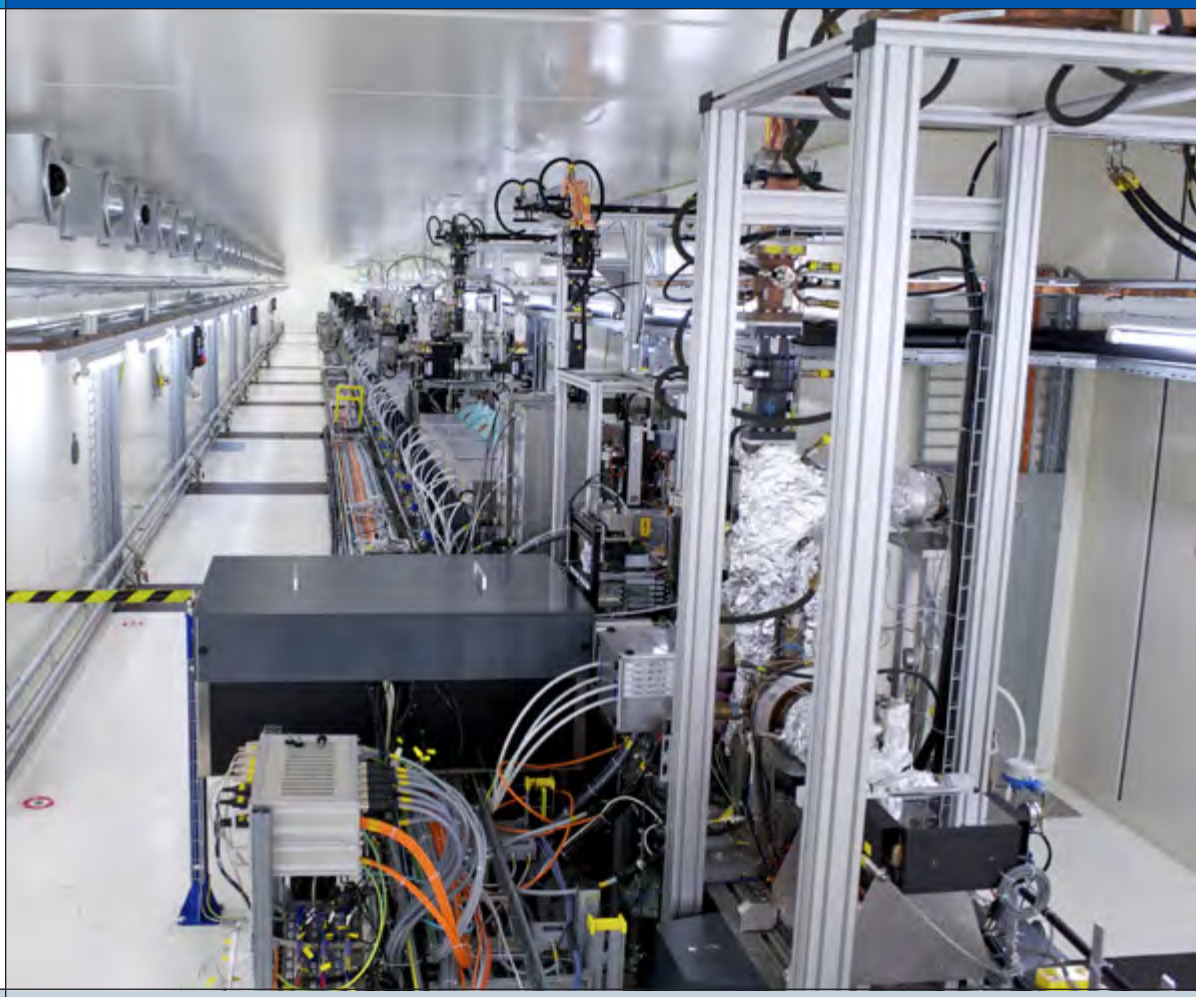

PSI Bericht Nr. 10-05
Juli 2010

Cover figures descriptions

Overview in the tunnel of the SwissFEL injector test facility in July 2010 during the assembly phase.

Editor

Marco Pedrozzi

With contributions from:

V. Arsov
B. Beutner
M. Dehler
A. Falone
W. Fichte
A. Fuchs
R. Ganter
C. Hauri
S. Hunziker
R. Ischebeck
H. Jöhri
Y. Kim
M. Negrazus
P. Pearce
J.-Y. Raguin
S. Reiche
V. Schlott
T. Schietinger
T. Schilcher
L. Schulz
W. Tron
D. Vermeulen
E. Zimoch
J. Wickström

Table of contents

1 Introduction

The SwissFEL X-ray FEL project at PSI, involves the development of an injector complex that enables operation of a SASE FEL at 0.1–7 nm with permanent-magnet undulator technology and minimum beam energy, i.e., a cost-effective way to obtain laser-like radiation in the X-ray spectral region. In order to extensively study the generation, transport and time compression of high brightness beams and to support the component developments necessary for the XFEL project, PSI is presently planning a flexible 250 MeV injector test facility.

The injector pre-project is motivated by the challenging electron beam requirements necessary to drive the SwissFEL accelerator facility. First, the source and the injector linac determine the minimum achievable emittance of the electron beam after full acceleration and therefore the maximum beam brightness at the undulator. Second, the shot to shot stability of the FEL radiate power, his arrival time and spectrum depends strongly on the injector fluctuations which must be kept below a reasonable level. More details about specifications for the Free Electron Laser project can be found in the SwissFEL conceptual report [1].

2 Mission of the test facility

Generally the injector test facility must fulfill two main purposes. Firstly it must provide a tool to benchmark the performances predicted by the simulation codes and to demonstrate the feasibility of a compact Free Electron Laser. Secondly it will be the ideal platform to develop and test the different components/systems and optimization procedures necessary to operate later SwissFEL. In more detail we can list the missions of the facility as follow:

- The facility provides the necessary background to analyze the generation and propagation of high brightness beams compatible with the specification of SwissFEL. The diagnostic system is designed for a careful comparison with the Beam Dynamic Simulations:

  – The machine is designed for optimal emittance compensation at 250 MeV (invariant envelope matching technique)
  – A compression chicane is implemented at 250 MeV and optimized for minimum emittance growth.
  – Monitoring of the beam position and size with a resolution ≤10 µm along the entire machine (integrated BPM-screen monitors).
  – The diagnostic line after the compression chicane allows measurements of projected and sliced parameters (phase space characterization).

- During the injector commissioning and optimization the operator crew will elaborate, optimize and automize the commissioning and operation procedures which will later be transferred to SwissFEL:

  – QE measurement procedure
  – GUN-Laser-Solenoid alignment procedure
  – Beam Based Alignment procedure
  – Projected parameter measurements
  – Slice parameter measurements
  – Emittance optimization procedure (invariant envelope matching)
  – Compression optimization (CSR studies)
  – Orbit feed back, bunch length feed back, energy feed back

- The short and bright beam bunches delivered by the injector are used to support component developments: the key hardware components are developed and tested in order to reach the required functionality for SwissFEL:

  – Gun tests (gun developments, photo cathode surface preparation)
  – RF (phase and amplitude stability – femtosecond synchronization)
  – Diagnostics (BPM and screen resolution, slice parameters, bunch length monitor, arrival time monitor, charge monitors)
  – Laser (longitudinal and transverse shaping, wave length emittance tuning & stability)
  – Mechanical stability and alignment concept (Girder concept and support systems)
  – Controls (expert panels and operations panels)
  – Fast linac tuning and restore procedures

- Establish commissioning/operation experience and consolidate the know how for SwissFEL commissioning and operation.

3 Performance Goals

The scientific objectives of the injector facility can generally be summarized in terms of beam performance, component functionality, machine stability and reliability. The primary objective of the installation is to explore the generation of high brightness beams according to the requirements of SwissFEL. The beam parameter range to be reached and explored with the injector is directly based on SwissFEL baseline specifications.

The feasibility of a compact SwissFEL has been analyzed via start to end beam dynamics simulations including the FEL undulator lines. To establish a robust baseline concept the injector has been designed starting from the experience accumulated with advanced RF photo-cathodes similar to the LCLS photo-cathode source [2]. Nevertheless the option of integrating later the innovative Low Emittance Gun (LEG) presently under investigation at PSI [3] has been kept. The typical parameter

SwissFEL Parameter Range			
Operation mode	Long pulse	Short pulse	Ultra short pulse
Single bunch charge (pC)	200	10	10
rms spotsize of gun drive laser (μm)	270	100	100
FWHM pulse length of gun drive laser (ps)	9.9	3.7	3.7
Peak current at the cathode (A)	22	3	3
Maximum number of bunches / pulse	2	2	2
Minimum bunch spacing (ns) / pulse	50	50	50
Normalized projected emittance (mm.mrad)	0.65	0.25	0.45
Normalized slice emittance (mm.mrad)	0.43	0.18	0.25
rms slice energy spread (keV)	350	250	1000
Peak current at the entrance of undulator (kA)	2.7	0.7	7
Beam energy for 0.1 nm (GeV)	5.8	5.8	5.8
rms photon pulse length at 0.1 nm (fs)	12	2.1	0.3
Number of photon at 0.1 nm ($\times 1 \cdot 10^{9}$)	24	1	4
Saturation length (m)	45	50	30
Bandwidth ($x1 \cdot 10^{-4}$)	3.1	2.5	5
Maximum repetition rate (Hz)	100	100	100

Table 1: Parameter range in the SwissFEL baseline.

Parameter	Input parameter and simulated performances at 250 MeV		
Charge (pC)	200	100	10
Laser diameter on cathode (μm)	1080	857	400
Laser pulse length FWHM – uniform distribution (ps)	9.9	7.9	3.7
Peak current on cathode (A)	22	14	3
Thermal emittance (mm.mrad)	0.195	0.155	0.072
Core normalized slice emittance before/after BC (mm.mrad)	0.32/0.33	0.213/0.213	0.078/0.078
Normalized projected emittance before BC (mm.mrad)	0.35	0.233	0.095
Normalized X/Y projected emittance after BC (mm.mrad)	0.379/0.35	0.268/0.233	0.104/0.096
RMS Bunch length before BC (ps)	2.8	2.23	1.05
RMS Bunch length after BC (fs)	193.3	117.6	33.2
Peak current after BC (A)	352	285	104
RMS beam size on OTR in 3rd FODO cell (μm)	55	35	14

Table 2: Input beam parameters at the electron source and simulated output at 250 MeV.

range of the SwissFEL is summarized in Table 1. Particularly challenging is the extremely low transverse emittance necessary to guarantee the electron beam transverse coherence during the lasing process at 0.1 nm.

The results of the beam dynamic simulations for the injector test facility are briefly summarized in Table 2. According to our analysis the test facility should deliver a beam well matched to the FEL specifications shown above with reasonable margin to take into account possible emittance dilution effects along the main linac.

Due to the relatively low energy and the initial beam manipulations the FEL injector up to the first compression chicane is one of the most critical section of the overall accelerator complex. The RF phase fluctuations, the alignment errors and mechanical vibrations of the components and the synchronization systems can induce large shot to shot fluctuations of the FEL radiated wave length and power. Energy, arrival time, orbit and peak current must thus be kept within severe tolerances to comply with the experimental requirements at the FEL photon beam lines. These tolerances imply not only extremely stable RF and synchronization systems but also the capability of diagnosing with sufficient resolution and correcting dynamical errors. For this reasons the Injector will be used as platform for the diagnostic developments and to test the feed back methods to be later applied to SwissFEL. Table 3 illustrates briefly typical tolerances for SwissFEL that will be explored during the operation of the injector test facility and which imply a staged R&D effort to reach the required final functionalities of all components [4].

Typical tolerances for SwissFEL	
Goal arrival time stability (fs)	*20*
Goal relative energy stability at 2.1 and 5.8 GeV	*$5 \cdot 10^{-4}$*
Goal peak current stability at the undulator (%)	*5*
Injector tolerances	
Photo cathode laser pointing stability (μm)	<10
Photo cathode laser energy stability (%)	0.84
Photo cathode laser jitter (fs)	55
Charge stability (pC)	1.68
S-band RF phase stability (deg)	0.022
S-band RF amplitude stability (%)	0.04
X-band RF phase stability (deg)	0.033
X-band RF amplitude stability (%)	0.2
Main Linac tolerances	
C-band RF phase stability (deg)	0.315
C-band RF amplitude stability (%)	0.1
Undulator line quadrupole alignment (μm)	3
Orbit stability in the undulator section (μm)	1

Table 3: Typical tolerances for the SwissFEL.

4 Accelerator layout

4.1 Overview

As shown in Figure 1 the electrons emerge on the left side of the facility from an S-band RF photoinjector. A booster linac based on normal conducting S-band RF technology increases the energy up to approximately 270 MeV generating simultaneously the necessary energy chirp for the magnetic compression. In front of the magnetic chicane a fourth harmonic X-band cavity, phased for deceleration, linearizes the longitudinal phase space for optimal bunch compression suppressing the formation of peaks in the head and tail of the current profile. The last drift section is dedicated to the beam characterisation.

The design of the beam-optics of the 250 MeV linac relies on the technique of so-called emittance compensation [5, 6, 7], where space-charge forces are carefully used via a beam refocusing to control the natural evolution of the emittance in the first few meters of the accelerator.

It is important to appreciate that the dynamics of high brightness beams in the initial phase of acceleration are highly dominated by space-charge forces. With respect to this point the SwissFEL injector doesn't differ substantially from other injectors designs. A good measure

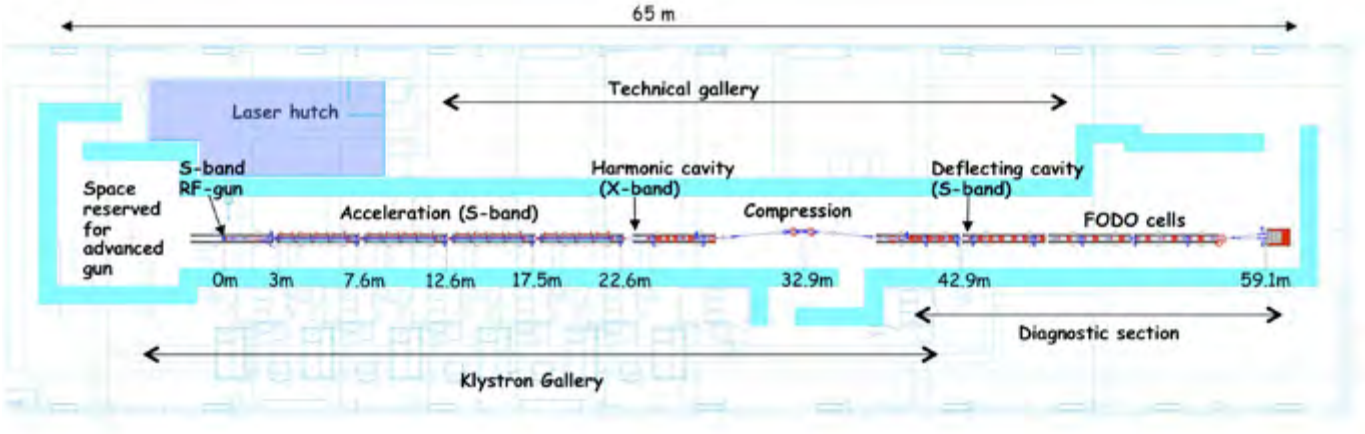

Figure 1: General layout of the 250 MeV injector facility.

to evaluate the dominance of space-charge is the so-called laminarity parameter ρ [8], which reflects the ratio in influence on the beam-dynamics between space-charge and emittance

$$\rho = \frac{I\sigma_{xy}^2}{2\gamma I_A \varepsilon_n^2} \qquad (4\text{-}1)$$

where I, σ_{xy}, γ, ε_n denote the current, the beam radius, the Lorentz factor associated with the beam energy, and the normalized beam-emittance, respectively. The laminarity parameter is scaled with the Alfèn current $I_A \approx 17$ kA. The high brightness photoinjectors considered for FEL or collider applications are usually largely space charge dominated. The parameters quoted in Table 4 for three different FEL photoinjectors lead to ρ factors at low energy well above unity, indicating a predominant influence of space charge on the beam dynamics. From the theory of emittance compensation [9], it follows that the space-charge forces can be controlled, provided sufficient care is given to the design of the accelerating system.

	SwissFEL		XFEL [10]	LCLS [11]
Bunch charge (nC)	0.2	0.01	1	1
Peak current (A)	22	3	50	100
Gun peak gradient (MV/m)	100	100	60	120
rms beam radius at matching point (mm)	0.3	0.1	1	0.41
Beam energy at matching point (MeV)	6.6	6.6	6.6	6.4
Normalized slice emittance (mm.mrad)	0.33	0.08	0.9	0.9
Beam brightness (A/mm^2mrad^2)	404	940	123	247
Laminarity parameter	38.4	9.9	130.5	45.1

Table 4: Laminarity parameter of the central slices for different photoinjectors estimated at the injection in the first accelerating structure following the electron source.

It is also important to keep in mind that in these regimes the required optics of the accelerator is dominated by the space-charge density of the electron beam. This has two important consequences:

- The beam-optics design of the linac must be optimized for a so-called working-point, which is defined by the bunch-charge and temporal profile of the bunch at each location along the machine. For the 250 MeV linac, the starting point is defined by the electron source parameters as specified in Table 2. However, the linac design presented in the following part of this chapter may be adapted to other source parameters. Generally, such an adaptation requires both a readjustment of the fields and location of solenoids, accelerating structures, etc. For practical reasons the design is chosen such that a large range of working points can be adapted without changing the location of the hardware.
- In the space charge dominated regime, it is important to maintain the circular symmetry of the electron beam since this provides an equal space-charge density in the horizontal and vertical plane. By contrast, a non-circular beam requires a machine design that provides a separate solution for the horizontal and vertical plane simultaneously. For this reason, all beam elements maintain the circular geometry at low energy where space-charge forces become dominant. Therefore the focusing in the linac section includes only solenoids. Quadrupoles are permitted in special combinations at the high-energy end of the linac, where space-charge forces are less dominant.

4.2 Electron source

To establish a robust baseline concept for the SwissFEL we decided first to concentrate our investigations on an electron source topology based on state of the art RF photo-injectors benefiting from the progress accumulated in the two last decades. Particularly encouraging in this field are the recent results achieved at LCLS [12] which complies with the specification of the SwissFEL. For the commissioning of the 250 MeV injector, an existing RF photocathode electron source will be used until a new electron source with higher performances, presently under development, will be ready (LEG [13] or advanced RF-photo injector). According to simulations (see Section 5) and recent experimental measurements, an injector based on a standard RF photo-cathode can already reach a slice emittance near to 0.3 mm.mrad.

The operation of the 250 MeV test injector will start with the CTF3 gun number 5 [14, 15], kindly lent by CERN to PSI. This RF-photo injector is a 2.5 cell standing wave cavity that was originally developed for high current operation at the CLIC test facility. The first half cell is overmoded in order to store enough RF energy to compensate beam loading effects, while the rear wall is

shaped in order to provide some additional focusing (Figure 2). Two RF coupling apertures are symmetrically located on the external wall of the last cell. The symmetric coupling will suppress the dipole component of the accelerating field in the last cell but no racetrack geometry was adopted to minimize the residual quadrupole component. A RF field probe pick up and frequency tuners are available on each cell.

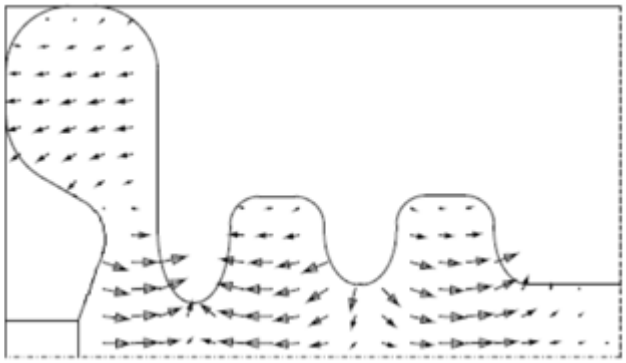

Figure 2: Cross section of the CTF gun number 5.

Following delivery, the cavity has been characterized at PSI to verify the RF parameters and the field profile. The measured values are summarized in Figure 3.

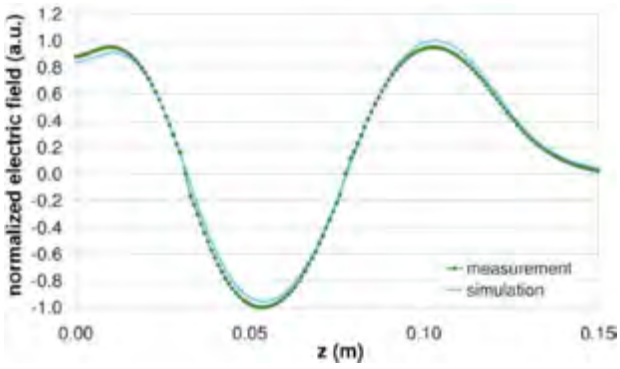

f_4	2998.725MHz
Q_L	7591
Qo	16153
β	1.13

Figure 3: RF parameter of the CTF3 gun number 5 measured at PSI. The field profile has been measured with the bead-pull technique.

The high power behavior of the cavity has been tested during one week in the SLS linac bunker (Figure 4). The nominal gradient of 100 MV/m was reached with a forward input power of 21 MW, and a temperature of the cavity of 47 °C [16].

Figure 4: The CTF gun number 5 in the SLS linac bunker during the high gradient tests.

According to the start to end simulations (see paragraph 5) the CTF 3 gun performs sufficiently well to deliver beam charges and emittances within the SwissFEL specifications. Nevertheless this source is not fully compatible with the operation modes foreseen for the FEL facility. First of all, the tuners overheat for repetition rates above 10 Hz and the overall cooling is not compatible with 100 Hz operation; secondly the effect of the quadrupole kick in the last cell on the final emittance has not been evaluated; and finally the cathode plug system in the first half cell is a weak point concerning dark current. For these reasons a procurement program for a new photo-injector has been initiated. The goal is to produce a new gun to be delivered by mid of 2011. The design strategy is based on an existing state of the art photo injector (LCLS and PHIN [17]). The cooling scheme will be modified to allow operation at a repetition rate of 100 Hz, and the mechanical assembly optimized in order to facilitate the cathode replacement for easier cathode surface treatments investigations.

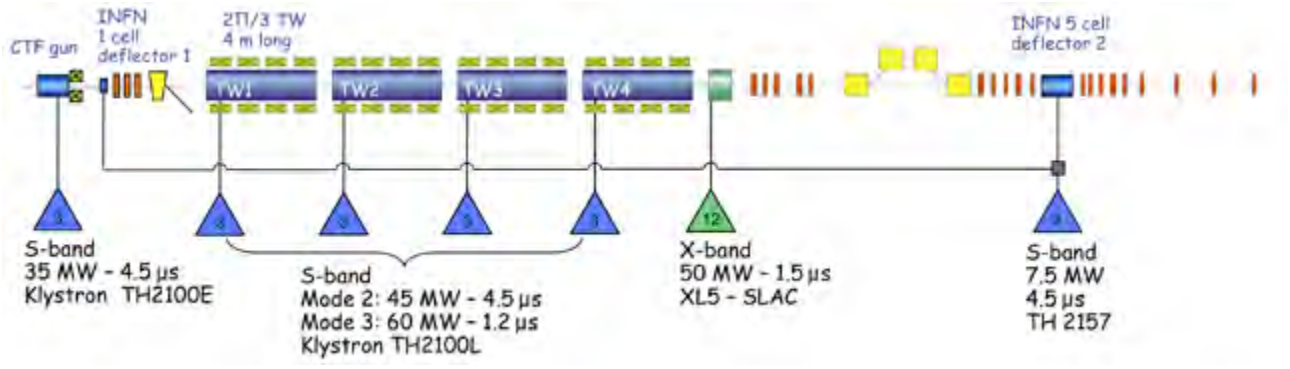

Figure 5: General layout of the Rf systems for the 250 MeV injector test facility. The operational modes of the klystrons are described in Table 8.

4.3 RF systems

4.3.1 General description

The general layout of the RF system is shown in Figure 5. The accelerator starts with the S-band RF-photoinjector described in section 4.2. A booster linac composed of four S-band structures, 4 m long, provide the required acceleration and energy chirp for the magnetic compression. A 12 GHz cavity is placed in front of the compression chicane for linearization of the longitudinal phase space. Two additional S-band deflecting cavities are implemented for diagnostics purposes in order to characterize the longitudinal phase space and slice parameters of the beam.

For maximum flexibility each accelerating structure will be powered by a dedicated power station. This choice allows a fine control of the RF focusing (gradient optimization) for optimal invariant envelope matching avoiding any cross talk between cavities. SLED compressors have not been considered for the initial phase to suppress any additional complication. The modulator and klystron can nevertheless be operated in a short pulse mode for a maximum gradient test (25 MV/m) and long pulse mode (45 MW) for a possible later installation of a SLED compressor system.

4.3.2 Accelerating structures

Booster linac

The booster linac consists of four constant gradient $2\pi/3$ travelling wave accelerating structures separated by a short drift where corrector, BPM and screen monitor are situated. The cavity RF design is based on the Linac II DESY structures and was re-optimized, compromising between maximum shunt impedance to decrease the power requirement at 25 MV/m and short range wakefield considerations. For small correction of the transverse focusing each cavity is surrounded by four 70 cm long solenoid magnets.

The design parameters of the S-band accelerating structures are summarized in Table 5.

Operating frequency at 40 °C (MHz)	2997.912
Phase advance	$2\pi/3$
Maximum total length flange to flange (mm)	4300
Number of cells	122
Operating temperature (°C)	38 – 42 ±0.1
Input coupler: Double-feed type	racetrack geometry
Output coupler Double-feed type	racetrack geometry
Nominal accelerating gradient (MV/m)	20
Maximum accelerating gradient (MV/m)	25
Shunt impedance per unit length (MΩ/m)	62
Peak power for 25 MV/m (MW)	57
Filling time (μs)	0.955
RF pulse length at 60 MW (μs)	1.2
Maximum RF pulse length at 45 MW (μs)	4.5
Maximum pulse repetition rate (Hz)	100
Material of the cavity	Cu-OFE
Material of the flanges, supports and cooling connectors	316LN
Concentricity tolerance (μm)	± 150
Design pressure of the cooling channels (Bar)	16

Table 5: RF parameters for the booster cavities of the 250 MeV injector. The nominal accelerating gradient depends on the position of the structure and ranges from 10 to 21 MV/m as described in paragraph 5.2.

Parameter	Dimension
p (mm)	33.333
t (mm)	5
r (mm)	10
a (mm)	12.695 9.31

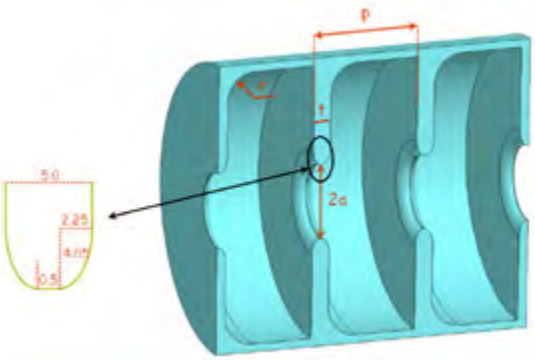

Figure 6: Detail of the iris design of the booster cavities and 3D model of the wave guide system at the input coupler (only the first cell is shown here).

The iris design has been optimized introducing an elliptical shape to reduce the maximum surface electric field (Figure 6). The iris radius "a" ranges from 12.695 mm at the cavity entrance down to 9.31 mm at the cavity end. The input and output coupler cavities have been symmetrized with dual feed and racetrack geometry. The ratio between maximum surface electric field and accelerating field is described in Figure 7.

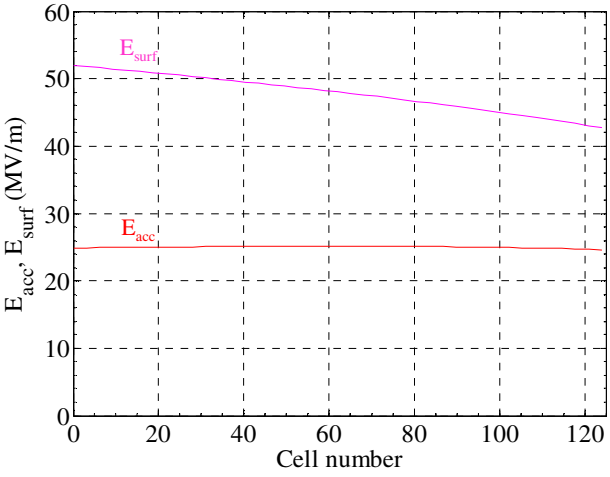

Figure 7: Accelerating field and maximum surface field along the booster cavity for 25 MV/m accelerating gradient.

The X-band harmonic cavity

The X-band harmonic cavity is a modified SLAC H75 structure. This structure is being developed in collaboration with CERN where the cavity will be tested for high gradient applications within the CLIC high gradient R&D program. Two cavities will be manufactured for PSI and two for the FERMI project. The cavity is a constant-gradient un-damped travelling wave structure with $5\pi/6$ cell-to-cell phase advance and 72 cells, (including the matching cells) [18]. The active length is 750 mm.

The cavity will be operated typically at peak gradient of 21.2 MV/m resulting in a total decelerating voltage of approximately 16 MV. The iris aperture (see Figure 8) ranges from 4.993 mm down to 4.107 mm. With such a small aperture this cavity will dominate the impedance budget of the entire linac. Misalignments larger than 10 µm can generate large transverse kicks with severe consequences on the final emittance. For this reason cell numbers 36 and 63 have been radially coupled to four wave guide systems (Figure 9) to extract dipole mode signals which will give an indication about the cavity misalignment and optimum beam positioning.

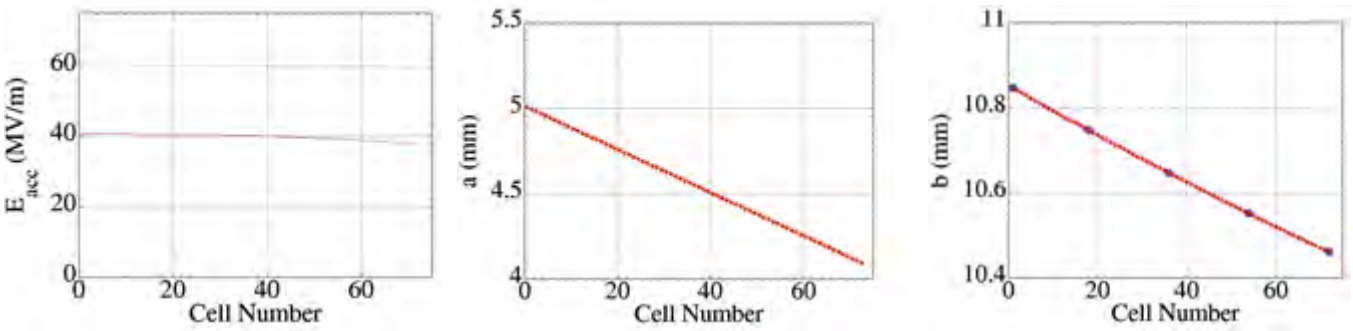

Figure 8: Gradient, iris radius and cell radius along the harmonic X-band cavity.

A mode launcher will be used to couple the RF power into the cavity and a similar structure will be implemented at the end of the structure to couple out the residual power (Figure 10).

The manufacture process will require a machining precision below 2 µm. According to the experience accumulated at CERN and SLAC in this field, such specification can be reached with modern temperature and vibration stabilized precision-machining tools

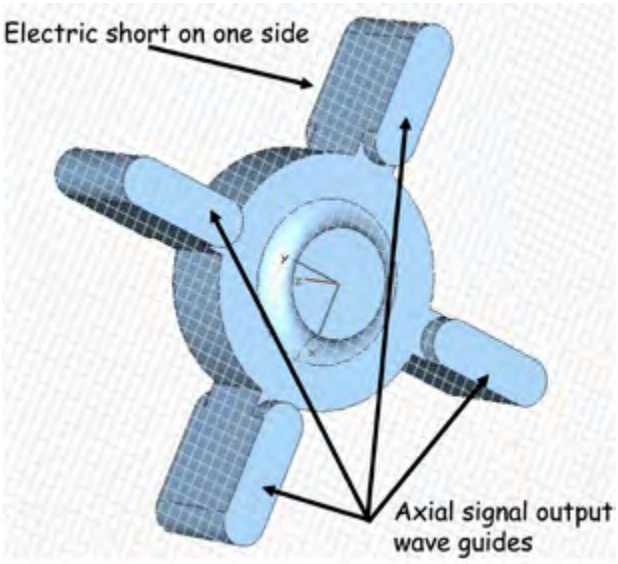

Figure 9: Special cell design with output ports for dipole mode monitoring.

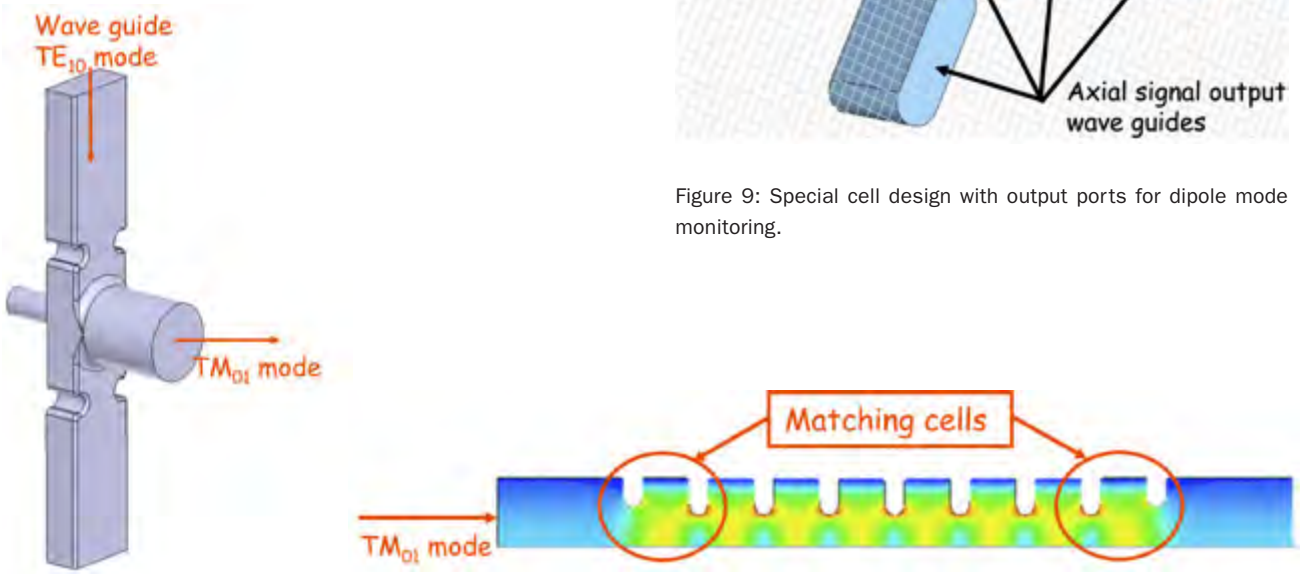

Figure 10: X-band cavity 3D model of the mode launcher and EM simulation of the input/output matching cells with electric field amplitude.

RF deflectors

The first deflecting cavity at low energy will be a single cell pill box cavity developed in collaboration with INFN. A wave guide port will be used as input coupler and a small antenna as a pick up. The RF parameters are summarized in Table 6.

No. of Cells	1
Frequency (MHz)	2997.912
Nominal/Maximum deflecting voltage (kV)	300/440
Nominal/Maximum input power (kW)	90/200
Repetition rate (Hz)	100
Filling time (µs)	~0.8
Nearest mode – different polarity (MHz)	50
Length flange to flange (m)	0.1
Quality factor – Q0	~15000
Shunt Impedance deflecting mode R (MΩ)	0.5
Aperture Beam pipe (diameter) (mm)	38
Working temperature	40°
Temperature range (°C)	35 – 50
No. Pickups	1

Table 6: Specification fort the low energy one cell deflector.

The high energy deflector is scaled from the structure developed for the SPARC project [19]. It will be manufactured by INFN within a collaboration framework with FERMI at ELETTRA and PSI. The cavity is a 5 cell standing wave structure (see Figure 11); the operating mode is the $TM_{110}.\pi$ like hybrid mode. The RF parameters of this structure are summarized in Table 7.

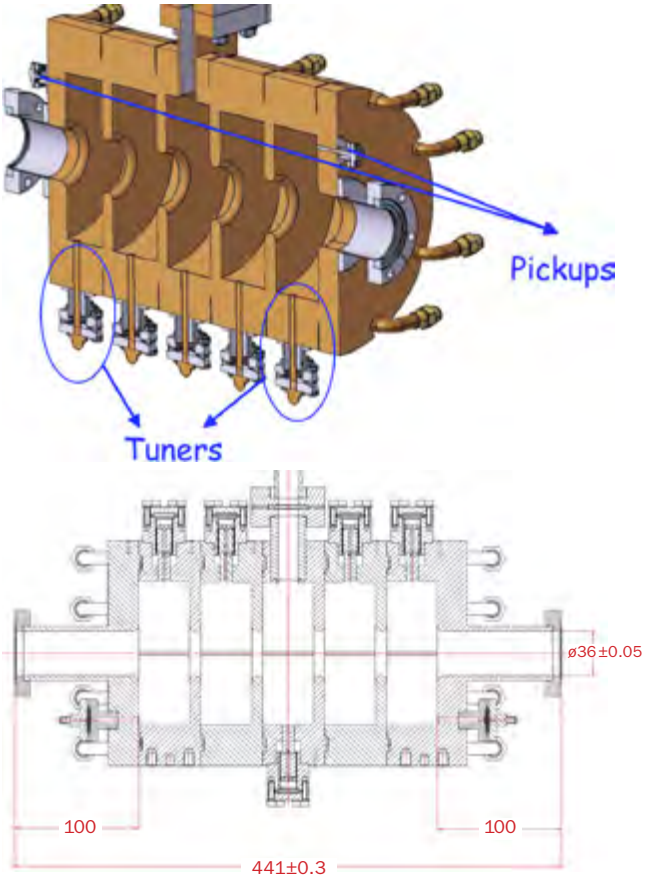

Figure 11: 3D model of the deflecting cavity designed by INFN for the FERMI project and the PSI version with the tuners displaced on the upper side.

No. of Cells	5
Frequency (MHz)	2997.912
Nominal/Maximum deflecting voltage (MV)	4.5/4.9
Nominal/Maximum input power (MW)	4.2/5
Operating mode	π
Repetition rate (Hz)	100
Filling time (μs)	~0.8
Nearest mode – different polarity (MHz)	50
Length flange to flange (m)	0.5
Quality factor – Q0	~15000
Shunt Impedance deflecting mode R (MΩ)	2.4
Aperture Beam pipe – diameter (mm)	38
Working temperature	40°
Temperature range (°C)	35 – 50
No. Pickups	2

Table 7: Specification for the 5 cell RF deflector to be installed at 250 MeV.

4.3.3 Power systems

The power modulators provide the high voltage pulsed power for the klystron amplifiers. These different sources are characterized by their peak power, pulse width, and high voltage and current capabilities. The three different klystron configurations in the FEL injector and accelerators, together with the maximum electrical parameters of the modulator power sources are given below in table 8.

Modulators that provide this high power are connected to the klystron loads through low leakage inductance and low stray capacitance high voltage step-up pulse transformers. The flat top of the voltage pulses produced are approximately equal to the RF pulse width of the klystron. The modulator energy efficiency is mainly determined by the rise and fall times of the voltage pulses, which will be approximately 1 μs and 2 μs (10 to 90 %) respectively.

The primary energy storage in each modulator can be either a pulse forming network (PFN) or switched capacitors. The PFN line type modulator method (Figure 12 and Figure 13) provides a fixed pulse width voltage pulse having a source impedance that is matched to the klystron impedance. The stored energy in the PFN is made just sufficient to satisfy the klystron load requirements. In this case the high voltage switch on the primary side of the pulse transformer needs to be only an ON device such as a Thyratron or a Sylicon Controlled Rectifier (SCR) assembly.

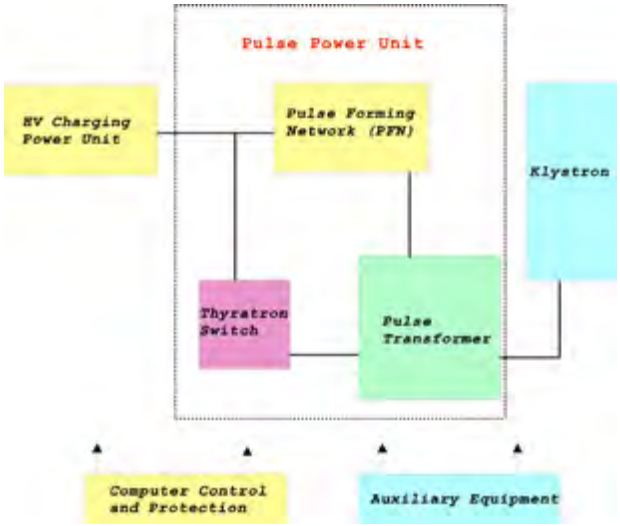

Figure 12: Line type modulator block diagram.

	3 GHz RF gun	3 GHz Linac – mode 1 to 3			12 GH	3 GHz Deflector	Unit
RF Peak Power	30	30	45	60	50	7.5	MW
RF Average Power	15	4.5	22.5	9	5	3.75	kW
Peak power klystron	71.4	69.7	104	146	107	15.7	MW
Average power klystron	53.1	19.6	65.2	42.5	26.5	10.2	kW
Klystron voltage range	266	261	307	351	410	148	kV
Klystron current range	268	267	340	416	262	106	A
Pulse flat top length	5	1.5	5	1.5	1	5	µs
Max pulse length (at 76%)	7.4	3.9	7.4	3.9	3.4	7.4	µs
Repetition rate	10–100	10–100			10-100	10-100	Hz
Flattop flatness (dV)	<±0.2	<±0.2			<±0.2	<±0.2	%
Rise rate (at 50 % voltage)	170/270	250–360			300-420	148	kV/µs
Fall rate (at 50 % voltage)	170/270	250–360			300–420	70–148	kV/µs
Amplitude stability	<±0.02	<±0.2			<±0.02	<±0.02	%
Pulse to pulse time jitter	<5	<5			<5	<5	ns
Pulse length Jitter	<±10	<±10	<±10	<±10			ns

Table 8: Modulator operational parameters of the klystron amplifiers.

In the second method (see Figure 14) where a capacitor discharge source is used, the stored energy has to be much larger than that required by the klystron load to ensure a voltage flat top region with a small percentage voltage drop. Additional protection is needed in this case to protect the klystron from receiving excessive energy from the storage capacitor in the case of a gun arc. This type of modulator commonly uses an IGBT solid-state ON-OFF switch to define the voltage pulse duration. Since these devices operate in a lower voltage region (3 to 6 kV) the step-up ratio of the pulse transformer needs to be a higher ratio than when a Thyratron switch is used (30 to 40 kV), and consequently requires a special transformer technology to ensure that the rise and fall times mentioned above can be achieved.

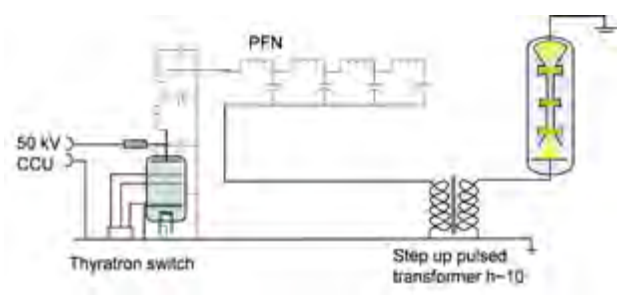

Figure 13: Typical scheme of a PFN modulator.

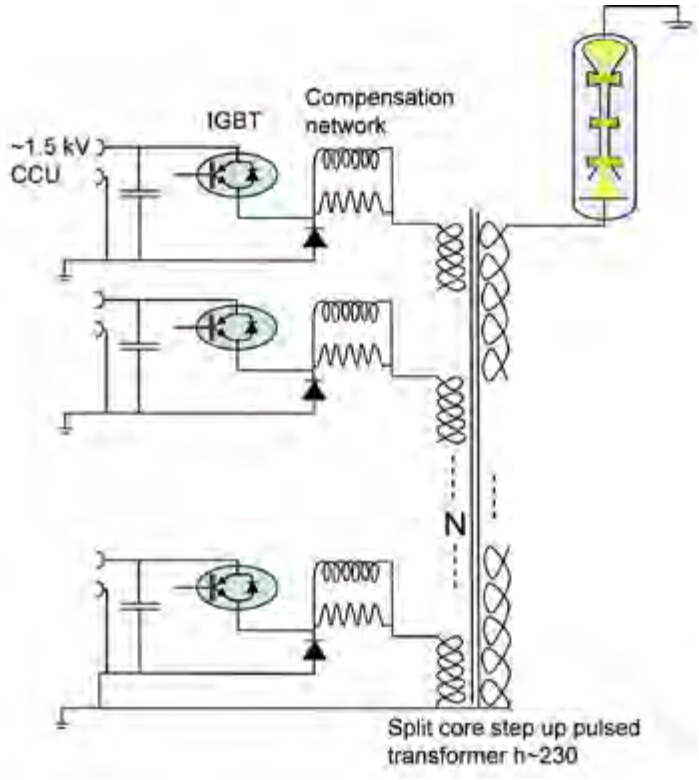

Figure 14: Electrical scheme of a solid state modulator.

Both these types of modulator have been investigated from the point of view of performance specification, reliability, maintainability and cost.

PFN modulators using conventional Thyratron switch technology are already in operation at the LEG test facility and the SLS machine, with known reliability and running experience. The main weakness of this approach, especially at high repetition rates, is the relatively short lifetime of the Thyratron switch (15'000 to 20'000 hours), which substantially contributes to the operation costs and reliability. The pulse behavior is fixed by the number of cells in the PFN and can be modified only by changing the capacitor configuration inside the modulator rack. The size of the components and the mechanical assembly is adapted to the relatively high voltages of the PFN line, fixing a physical limit to the compactness of the HV cabinet.

A low power solid–state modulator has been purchased for the LEG test facility introducing a new technology at PSI. This very compact device has been tested showing an extremely fast installation and commissioning procedure. The modulator is composed of a series of low voltage (~1 kV) switching modules connected in parallel to the step up transformer (see Figure 14). In general the solid state modulator tested at PSI presents the following advantages:

1. Compactness
2. Fast installation (only three main connection for electrical power, cooling and controls)
3. Modularity (the same switch modules can be stacked in different configurations, less spare components needed)
4. Reliability (70'000 hours without failures recorded by the suppliers, a few modules can fail without perturbing the modulator operation)
5. Adjustable pulse length
6. KHz repetition rate

At a comparable investment cost and based on the positive experience obtained so far, PSI has decided to use the solid state option for the injector test facility. The 3 GHz and 12 GHz modulators requires respectively voltages of 300 and 450 KV for a modulator peak power exceeding 140 MW. The design needs therefore a large amount of parallel operated solid-state IGBT devices with a high ratio step-up pulse transformer to handle the power that a PFN modulator with a single Thyratron or SCR assembly would handle. The new modulator concept consist in a "single rack" amplifier units integrating the tank, the water distribution and the power supplies for the klystron solenoids and heater (see Figure 15).

Figure 15: The high power modulator K2 from the company SCANDINOVA (10-60MW; 200-450 kV).

The klystron loads for the modulators are high gain RF power amplifiers that usually have a narrow bandwidth (10 MHz) at the fundamental frequency. The Thales TH2100 klystron shown below (Figure 16) is a typical example.

The RF output pulses from each klystron are transmitted via an RF window that is conditioned to operate with an SF6 gas pressure of about 2 bars. This electro-negative gas enhances the voltage hold-off capability in the presence of high forward and reflected power occurring in phase together at the window. If this should occur the used gas is recovered in a closed circuit system and the window volume is flushed with clean gas and re-filled.

Figure 16: High-power klystron amplifier TH2100.

As mentioned above the shot to shot RF phase and amplitude stability are particularly critical because they can potentially generate large FEL fluctuations (arrival time, power, wave length). Assuming a stable distribution

network, the RF phase and amplitude are mainly driven by the modulator voltage stability. To meet the FEL specifications (~0.01 deg RF) the relative voltage stability must be of the order of 10^{-5}. This will require an effort in ameliorating the capacitor charging scheme which usually reaches values one order of magnitude larger than the specified ones. To overcome this problem we plan at the injector facility, and in collaboration with the modulator suppliers, an R&D program to improve the performances of the presently commercial available hardware. Recent encouraging measurements of the achievable phase stability have been carried out at ELETTRA in the framework of the FERMI FEL project [20]. The experimental data reproduced below in Figure 17 indicates that a conventional PFN based S-band power plant is able to reach shot to shot stabilities below 0.1° peak to peak. A slow feed back system is nevertheless needed to correct slow phase fluctuations which might be induced by thermal drifts of the power plant components.

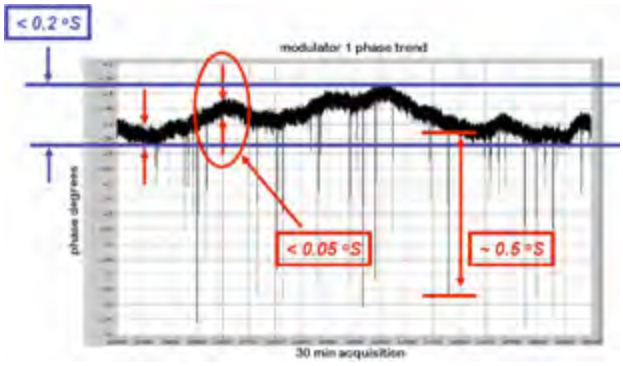

Figure 17: Phase stability of a conventional S-band power plant at ELETTRA (Courtesy of G. D'Auria).

4.3.4 Low level RF systems and synchronization concept

The purpose of the Low Level RF (LLRF) control system is to synchronize and regulate the RF fields in the accelerating cavities throughout the machine. For the injector, three different types of accelerating structures have to be controlled, namely

- 2.5 cell RF-photo injector, fundamental frequency, 3 GHz (standing wave structure)
- The booster accelerating structures, 3 GHz (traveling wave structure)
- The harmonic accelerating structure, 12 GHz (traveling wave structure).

Errors in amplitude and phase produce energy modulations, particularly if the beam is accelerated off-crest, which result in timing jitters from pulse to pulse after the compression chicane. The requirements in terms of amplitude and phase stability are given in Table 9. The table summarize the required RF tolerances needed at different stages of the injector commissioning and for the SwissFEL operation. The figures are based on preliminary tolerance studies for SwissFEL [3] and on further optimizations reported in the SwissFEL CDR [1].

	Gun alone	Injector without BC1	Injector with BC1	Swiss-FEL
S-band amplitude stability (%)	0.1	0.05	0.04	0.04
S-band phase stability (deg)	**0.3**	**0.05**	**0.022**	**0.022**
X-band amplitude stability (%)			0.2	0.2
X-band phase stability (deg)			**0.2**	**0.033**

Table 9: Estimation of the amplitude and phase rms stability requirements (rms) for the RF accelerating structures at different phases of the injector commissioning and for SwissFEL.

* timing stability of the driving laser for photoemission of 0.1 ps to 0.2 ps.

To fulfill these requirements several stages are foreseen. The basis for stable RF input powers to any of the accelerating structures are stable klystron modulators (see section 4.3.3). The promising results which are shown there indicate the need for a slow, pulse to pulse regulation of the input amplitude and phase. In case of systematic repetitive errors within the few microseconds long RF pulses a fast feed forward system could in addition reduce these perturbations. These tasks can best be achieved by digital feedback and feed forward systems. The latter especially has the potential to use adaptive algorithms in order to compensate systematic pulse to pulse distortions. It is therefore foreseen to implement the LLRF system as a digital system which is well integrated in the accelerator control system. A generic overview of the RF cavity control is depicted in Figure 18.

The Low Level RF Electronics concept is based on down converting any RF signals (3, 12 GHz) to a common intermediate f_{if} frequency of 46.84 MHz which is the 64th sub-harmonic of 3 GHz. These signals are digitized by 16 bit ADCs sampling with 125 MHz (24^{th} sub-harmonic

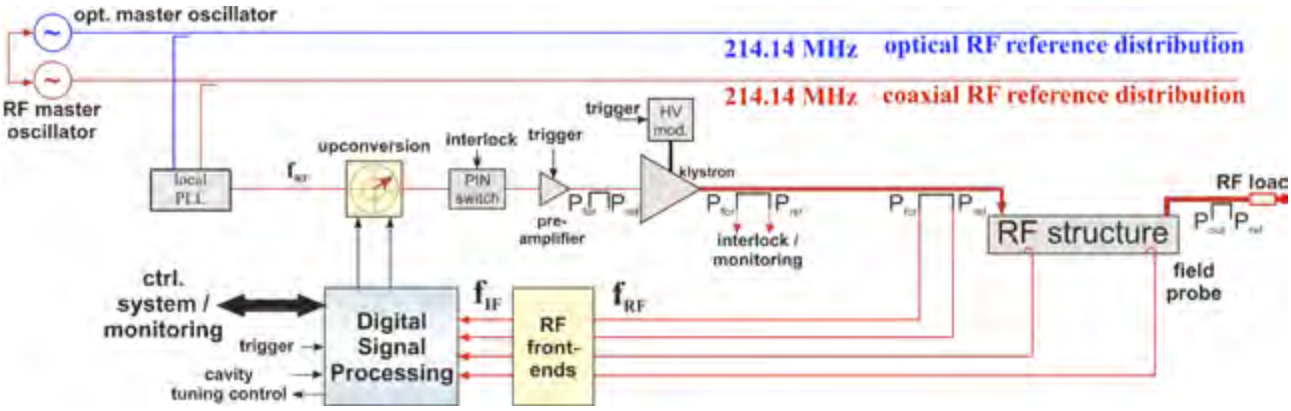

Figure 18: Generic LLRF system layout for the accelerating structures. For a standing wave cavity, with no field probe is available, the cavity field vector has to be calculated based on the measurements of the forward and reflected power.

of 3 GHz) synchronously with the Master Oscillator. On state-of-the-art FPGA platforms (Xilinx Virtex5) the in-phase and quadrature-phase components of the RF vectors are extracted by non-IQ sampling [21]. Digital pulse to pulse feedbacks and adaptive feed forward systems to compensate repetitive systematic distortions will maintain the very tight amplitude and phase stability requirements of the individual RF cavities. Vector modulators will control the drive signal to the high power klystrons. The I/Q input signals of the vector modulators are generated by 16 bit DACs driven by the same 125 MHz clock as the ADCs.

A required phase stability of 0.01 deg at 3 GHz corresponds to a temporal RF stability of approximately 10 fs making the overall synchronization scheme particularly challenging. The pulse to pulse RF stability will mainly be determined by the high voltage pulse to pulse stability of the modulators which has to be on the order of 10^{-5}. Although PFN based modulators have already reached this stability [22] the applied solid state based modulators have still to demonstrate this performance. Concerning the synchronization, all local oscillator, ADC and DAC clock signals are derived from the 3 and 12 GHz reference signals which are generated locally at each RF station by PLL systems locked to the distributed reference signal of 214 MHz. A temperature stabilized LLRF distribution system and an optical synchronization system will be installed in parallel (Figure 19). While the more robust RF-based system will guarantee machine operation with sub-50 fs peak to peak stability, the more sophisticated optical timing distribution will be tested during the injector operation aiming for sub-10 fs timing jitter. Details of the distribution system can be found in [23].

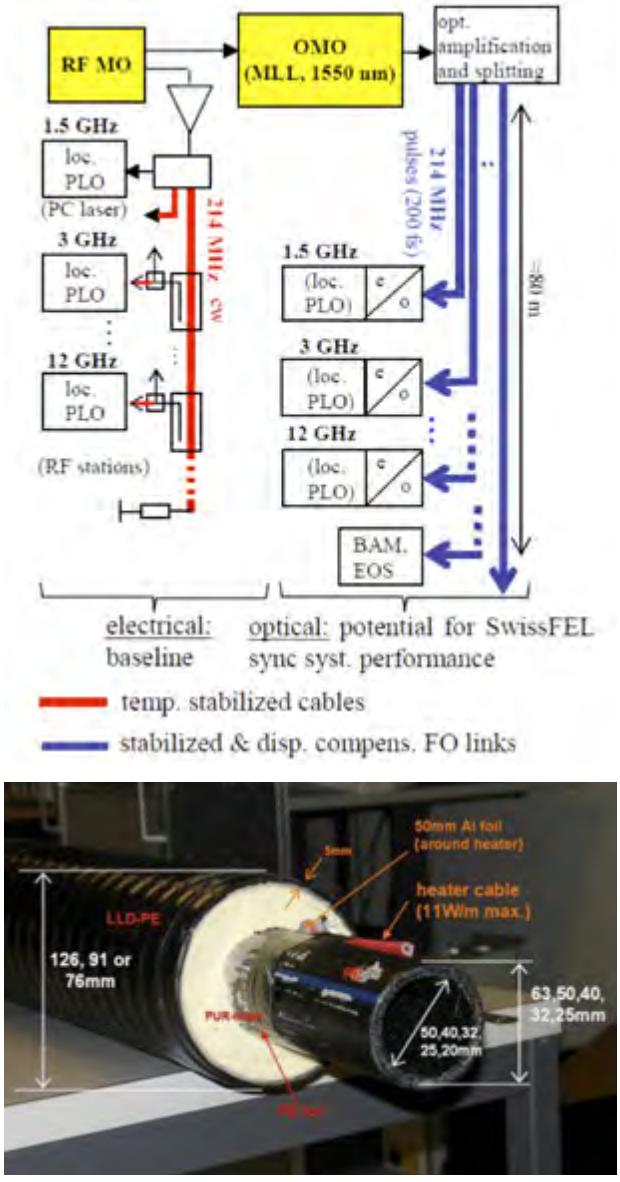

Figure 19: Simplified layout of electrical and optical reference distribution and temperature controlled cable pipe for the electrical distribution.

All drive signals for the klystrons and local oscillator frequencies for IQ detection are either generated by standard frequency multiplication/division techniques or by conversion of the optical signal of the synchronization laser link to an electrical RF signal. The Optical Master Oscillator (OMO) produces laser pulse trains with repetition frequency f_R = 214.4 MHz which generate a spectrum of all harmonics $n \cdot f_R$ at the output of a high bandwidth photo diode. Selecting the appropriate harmonics by bandpass filtering provides the desired RF frequency as a drive or local oscillator frequency. High frequencies above 4.5 GHz are most likely generated from the laser pulse spectrum by means of dielectric resonator oscillators (DRO) [24].

The RF gun cavity integrates field probes to extract the signal by means of bandpass filters. If a field probe should be omitted in order not to disturb the radial symmetry of the RF cavity the accelerating fields in the RF gun have to be calculated from the forward and reflected powers requiring precise calibration of these signals [25].

The frequency tuning of the RF cavities during operation will be accomplished by a temperature tuning system. The digital LLRF system will determine the detuning of the cavity from pulse to pulse. The LLRF systems have to analyze this information, calculate the necessary tuning change and set the new set-points for the temperature accordingly. A digital interface between the LLRF and the tuning system will provide the necessary communication. Standard cooling control units typically regulate the temperature within 0.1°C which corresponds to ~5 KHz for an S-band cavity. This causes a change in RF phase of about 2.6° (@3 GHz). A pulse to pulse LLRF feedback system is therefore compulsory to compensate temperature induced phase drifts and adjust the RF cavity phase to the required level of stability. Stabilization of a 1.6-cell RF gun operating at 2.86 GHz to less than 0.1° in phase and 0.1% in amplitude has been achieved so far with a similar digital LLRF approach [26, 27].

Following the modular approach for the LLRF system presented above only the analog front ends and the vector modulator have to be adapted to the different accelerating frequencies. The digital signal processing unit including the software will be mainly generic for all LLRF systems.

4.4 Diagnostics

4.4.1 Introduction – General Strategy for Beam Diagnostics

The 250 MeV X-ray Free Electron Laser (X-FEL) Injector Test Facility at the Paul Scherrer Institute will focus on the production, transport and diagnosis of high brightness electron beams. Using this facility the acceleration concept will be carefully investigated in order to demonstrate the feasibility of an economic X-FEL facility at PSI. Electron beam diagnostics will be designed to support the demonstration of the challenging SwissFEL Injector beam parameters and will thus need to provide high performance with excellent reliability and reproducibility. In addition, prototype developments for SwissFEL diagnostic systems will be made at the 250 MeV Injector Test Facility in order to re-engineer the chosen solutions for robustness and cost-effectiveness and to improve their performance and reliability at the same time. Information about absolute beam and lattice properties will be required for most of the measurements, while in some cases the online monitoring of relative beam parameters will support stable operation of the accelerator sub-sections. All diagnostic devices need to provide single-shot information. Measurement of projected and “sliced” beam parameters will be provided in the gun and pre-injector region (up to 8 MeV) and after bunch compression at full beam energy of 250 MeV. With regard to these general requirements and boundary conditions, the overall design concept for the electron beam diagnostics will aim for redundant delivery of information, accurate calibration of monitors and cross-check as well as cross-calibration of diagnostic devices (whereever possible). A modular configuration of components will provide sufficient robustness and reliability and permit at the same time enough flexibility to incorporate improvements, which may be necessary to validate the final accelerator performance and the SwissFEL beam parameters. Most of the (standard) monitors will be based on designs which have already been successfully utilized in the SLS (Swiss Light Source) pre-injector linac and at other linac-based FEL facilities. Adaptations to the specific needs and requirements of the SwissFEL project (especially the low charge and short bunch mode) as well as potential improvements regarding performance, simplicity of operation and reliability of the monitors will be incorporated in the designs at an early stage.

The personnel and competences required to provide state-of-the-art diagnostics for the 250 MeV Injector and the SwissFEL project will of course profit from the existing expertise of the PSI Diagnostics Section, specifically in the fields of beam position measurements and beam-based feedback systems. Experience with operational systems (such as e.g. the SLS digital beam position monitors [28], the fast orbit and multi-bunch feedbacks [29, 30] and the (optical) emittance monitor at SLS [31]) as well as new developments (such as the cavity BPMs and the "intra bunch train feedback" for the European XFEL) will support the efficient realization of high-quality monitors in these areas. Some of the competences for key diagnostics in linac-based light sources, however, have to be built up with the start of the 250 MeV Test Facility. Particularly longitudinal (bunch length and arrival time) and sliced diagnostics as well as timing and synchronization on a sub-100 fs (later sub-10 fs) level need to be efficiently introduced in order to realize high resolution monitors and operational diagnostics systems in due time. While basic concepts in these areas have been developed at PSI in the course of Doctoral studies and first results have been achieved at the SLS pre-injector LINAC [32] and for the SLS Femto-slicing project [33], a lot more effort and manpower has to be invested to reach the state-of-the-art at other LINAC-based radiation sources (such as FLASH and LCLS) and to provide the required measurements in a reliable manner and as a valuable support of accelerator commissioning and development.

Layout of Test Injector Diagnostics Sections

Following the general layout of the 250 MeV Injector Test Facility, the diagnostics sections can be divided in three sectors:

- the RF photoinjector,
- the S-band LINAC and bunch compressor and
- the high energy (250 MeV) diagnostics branch to analyze all final beam properties of the injector.

4.4.2 Low Energy Electron Beam Diagnostics

The low energy (<8 MeV) beam transport line between the electron gun and the first S-band accelerator structure has a length of almost 3 m, providing sufficient space for diagnostic monitors. Moreover, it is foreseen to test different electron gun settings over a wide range of beam parameters at the 250 MeV Injector Test Facility – starting with the CLIC 2 ½ cell RF gun, followed by

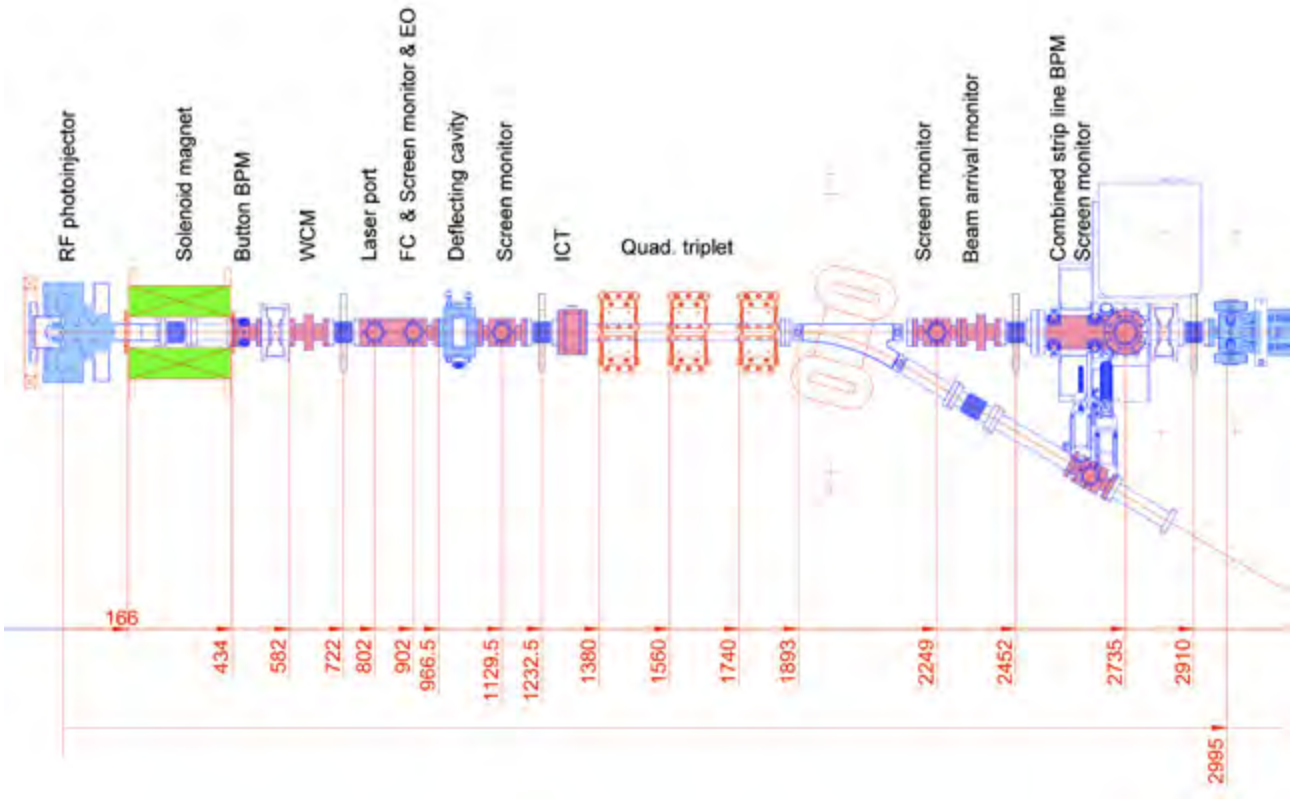

Figure 20: RF-gun with the first 3 m drift section and the beginning of the first accelerating structure.

an optimized PSI RF gun design. Thus, the possibility of a complete characterization of the projected and "sliced" electron beam phase space has been integrated in the low energy diagnostics line.

A set of four optical screen monitors allows the control, monitoring and optimization of the transverse beam envelope matching into the S-band injector linac. Due to the low beam energy YAG: Ce crystals will be used for the profile measurements. The readout system of the screen monitors consist of two selectable optical branches: the first, with a large useable area on the order of the beam pipe diameter, for electron beam optimization and halo detection providing medium spatial resolution of ~25 µm / pixel (projected pixel size). The second, with a small useable area of interest of up to 5 mm (maximum), providing high spatial resolution ~5 µm / pixel (projected pixel size) for beam measurements. A detailed description of the prototype screen monitor and optics design is given in [34]. A transverse (projected) emittance scan is possible by using the three quadupoles of the low energy line in combination with the 4th screen monitor directly in front of the 1st S-band linac structure. A set of horizontal and vertical slit masks as well as a "pepperpot" mask has been integrated in the combined resonant stripline BPM / screen monitor station directly in front the injector linac providing an alternative method to the quadrupole or gun solenoid scan for the determination of transverse beam emittance in case of a space charge dominated beam (200 pC operation mode). Imaging of the corresponding beamlets is possible by using the drift length of ~4.5 m to the next screen monitor station, located between the 1st and the 2nd S-band linac structure.

Two beam position monitors (BPM) – a button type (due to the restricted available space) and a 500 MHz resonant stripline [35] – are integrated in the low energy beam line for electron beam trajectory measurements. While the button type BPM pick-up provides only limited resolution of ~100 µm (especially in the low charge operation mode) at the exit of the gun solenoid, the resonant stripline BPM will be able to determine the transverse beam position with ~10 µm single-shot resolution [36]. By using the low energy corrector magnets, a beam position feedback for the entrance point of the 1st S-band linac structure will be implemented.

A coaxial Faraday cup, a wall current monitor and an integrating current transformer (ICT) [37] will be used to monitor the bunch charge and the charge profile within the gun RF pulse. While the coaxial Faraday cup and the wall current monitor allow the observation and optimization of possible dark current from the RF gun, the ICT can be used for monitoring the quantum efficiency of the photo cathode and for the implementation of a possible bunch charge feedback by keeping the gun laser intensity constant.

An electro-optical bunch length monitor [38] using the method of spectral decoding will be installed in a combined screen monitor / EO monitor station (CF40 diagnostics cube) at 2249 mm downstream of the photo cathode. Using a GaP bi-refringent crystal in the UHV beam pipe and an Yb-doped fiber laser at 1030 nm wavelength [39], the Coulomb field of the electron bunch can be probed with sufficient time resolution (<1 ps) to monitor the rectangular electron bunch profile with its 700 fs rise and fall time and 9.9 ps (FWHM) duration. In addition, this monitor allows the comparison of the longitudinal electron beam profile with the auto-correlation measurement of the longitudinal laser pulse profile to optimize the laser beam transport line from the laser hutch to the photo cathode in the accelerator bunker. The performance and stability as well as reproducibility criteria of this EO-monitor will be tested in the low energy gun region in order to provide effective single-shot bunch length information with similar systems at higher energies (250 MeV) and at shorter (sub-ps) electron bunch lengths before and after the bunch compressor.

Likewise, an electro-optical electron bunch arrival time monitor (BAM) will be implemented in the low energy beam transport line between the RF gun and the injector linac to monitor the beam arrival time with respect to a stabilized optical synchronization link using a commercial Er-doped fiber laser with extremely low (3.3 fs) jitter [40]. A high bandwidth (>15 GHz) pick-up consisting of four button electrodes (2 mm diameter) and four ridged waveguides has been designed to generate a fast (<100 ps slew rate) voltage pulse of about ±10 Vpp in both operation modes (button pick-up for 200 pC and ridged waveguides for 10 pC) of the Injector Test facility. While the electro-optical BAM in the gun region will provide information about the photo-cathode laser timing stability, the performance of two more BAMs, respectively in front of and behind the bunch compressor, will monitor the energy and RF amplitude (and phase) stability of the injector accelerator structures. In addition to the beam arrival time measurement, it is planned to compare the distribution of the 214 MHz reference signal (laser pulse repetition rate) over stabilized optical

links with a more conventional distribution using a RF microwave master oscillator and RF microwave components, in order to decide on the synchronization scheme for the final reference distribution of the SwissFEL.

The momentum and momentum spread of the electron beam can be measured through dispersion created by a dipole magnet (30° bending) in a spectrometer arm. Absolute momentum measurement is given by the geometry and calibration of the dipole and the subsequent drift length (600 mm). In order to maximize the momentum resolution of the spectrometer, the dispersive contribution to beam size should be large compared to the emittance contribution. This is achieved by use of the quadrupole triplet in front of the dipole, which provides a sharp horizontal focus at YAG:Ce doped screen, SME, and limits the beam size vertically. The setting for the focus is not known a priori, since space charge effects will perturb the beam transport matrix transformation, and the focus will be hard to find on SME where the beam is widened by dispersion. Therefore another screen, SCR20, is located in the non-dispersive, straight beam path with the same path length. The dipole MBND10 is a gradient free rectangular magnet, which behaves like a drift horizontally, so a focus produced at SCR20 and well observable there, will be moved to SME after switching on MBND10.

A single cell S-band transverse RF deflector has been designed in collaboration with INFN Frascati. More detailed information about the design and the RF specifications are given in the RF section of this report. The deflector will be installed for measurement of the electron bunch length as well as “sliced” (horizontal) emittance and sliced energy spread at 1000 mm downstream of the gun. The maximum deflecting voltage of 300 kV and the drift space (1700 mm) to the screen SCR20 in front of the 1st S-band accelerating structure will provide ~200 fs time resolution, which is sufficient to resolve the 700 fs rise and fall time of the longitudinal bunch profile in both operation modes (200 pC and 10 pC) of the Injector Test Facility. A quadrupole triplet can be used to increase the resolution of the longitudinal phase space measurements.

4.4.3 Linac and Bunch Compressor Diagnostics

Between each of the S-band accelerator structures combined BPM/screen monitor stations, consisting of a 500 MHz resonant stripline BPM and a YAG:Ce and OTR (optical transition radiation) screen, allows monitoring the electron beam position and to visualize the transverse electron beam profile. Two additional BPM/screen monitor stations will allow matching and position control of the electron beam through the X-band structure located donstream of the injector linac. The screen monitor station directly in front of the bunch compressor can be used in combination with the upstream quadrupoles to determine transverse beam emittance and Twiss parameters for correct matching into the bunch compressor. A beam position and angular feedback, which is driven by the BPM readings in front of the bunch compressor is used to provide stable beam trajectory conditions for any given bunch compressor setting. Transmission through the S-band linac can be measured with an ICT. An EO bunch length monitor applying the method of spectral decoding allows the online control and monitoring of the longitudinal charge distribution in front of the bunch compressor. A set of two EO beam arrival time monitors (BAM) – one in front of the bunch compressor and one directly behind the bunch compressor – can be used to determine the beam arrival time. The BAM signals can be used in a (slow) feedback loop to prevent beam energy drifts and to stabilize the RF amplitudes of the injector linac structures. The expected energy resolution from the BAM measurements is $\sim 4 \times 10^{-5}$, corresponding to <10 fs beam arrival time measurement resolution.

Two of the standard 500 MHz resonant stripline BPMs at the entrance and exit of the bunch compressor will be used to monitor the energy and energy stability of the electron beam. Although the BPMs are not located at maximum dispersion in the center of the bunch compressor (R_{56} of 430 mm) the expected position resolution of 10 µm and the R_{56} of 90 mm at the location of the BPMs will provide an energy resolution of $\sim 1 \times 10^{-4}$. The BPM performance will be compared to the BAMs, in order to determine the most suited energy and RF amplitude feedback configuration for later use in SwissFEL. A pair of horizontal slits in the center of the bunch compressor will be used to cut energy tails of the beam. A screen monitor directly behind the slits provides information about the energy spread induced by the off-crest acceleration in the S-band linac and the linearity of the

energy chirp achieved by the X-band structure. A synchrotron radiation monitor behind the third BC bending magnet provides the same information in a non-destructive manner for online monitoring and possible feedback applications. Coherent synchrotron radiation (CSR) in the mm-wave and THz spectral range will be coupled out from the fourth (last) bending magnet of the bunch compressor. The integral intensity will be measured with a Golay Cell or pyro-electric detector to control, monitor and optimize the compression of the electron bunches. The CSR-based compression monitor will also allow to find the correct phase setting of the S-band LINAC structures and might be used to implement a feedback on the RF phase settings of the linac.

4.4.4 High Energy Electron Beam Diagnostics

All electron beam parameters (projected as well as sliced beam properties), which are relevant for validating the RF Photoinjector performance and the acceleration (injector) concept for SwissFEL have to be measured at the end of the Injector Test Facility at 250 MeV beam energy.

A 5-cell transverse RF deflecting cavity (TDS), which has been redesigned by INFN Frascati to European S-band frequencies for use at the FERMI and the SwissFEL projects, will be installed in the diagnostics section behind the bunch compressor. More detailed RF specifications of this TDS are listed in the RF section of this report. Since the main purpose of the SwissFEL Injector Test Facility is focused on the optimization of components and accelerator sub-systems to obtain a high brightness, low emittance electron beam, a FODO lattice has been chosen to allow the measurement of the projected (TDS off) and "sliced (TDS on) horizontal emittance without changing the beam optics settings. A matching optics consisting of 5 quadupoles generates a vertical β-function of 20 m in the TDS providing efficient vertical deflection of the beam. Five more quadrupoles are used for matching into the three FODO cells with a total horizontal phase advance ψ_x of 165° (55° per FODO cell). The horizontal β functions of 5 m at the location of the 7 screen monitor stations, which are distributed along the FODO cells, provide a time resolution of ~20 fs respectively ~10 fs assuming up to 4.5 MV deflecting voltage and the desired beam emittances of 0.4 mm.mrad for 200 pC and 0.125 mm.mrad for 10 pC respectively. The TDS time resolution corresponds to ~10 slices along the 185 fs (rms) long bunch in case of the 200 pC operation mode, while in the short bunch (10 pC) mode only 3 slices can be visualized over the extremely short bunch length of ~30 fs (rms). A dipole magnet at the end of the diagnostics line can be used as a spectrometer to measure the projected and "sliced" energy distribution of the beam. The left side of figure 21 provides a schematic view of the 250 MeV diagnostics section including the horizontal (β_x) and vertical (β_y) β-functions as well as the beam dispersion η_x. The phase advances (ψ_x, ψ_y) along the FODO lattice are shown on the right side of Figure 1.

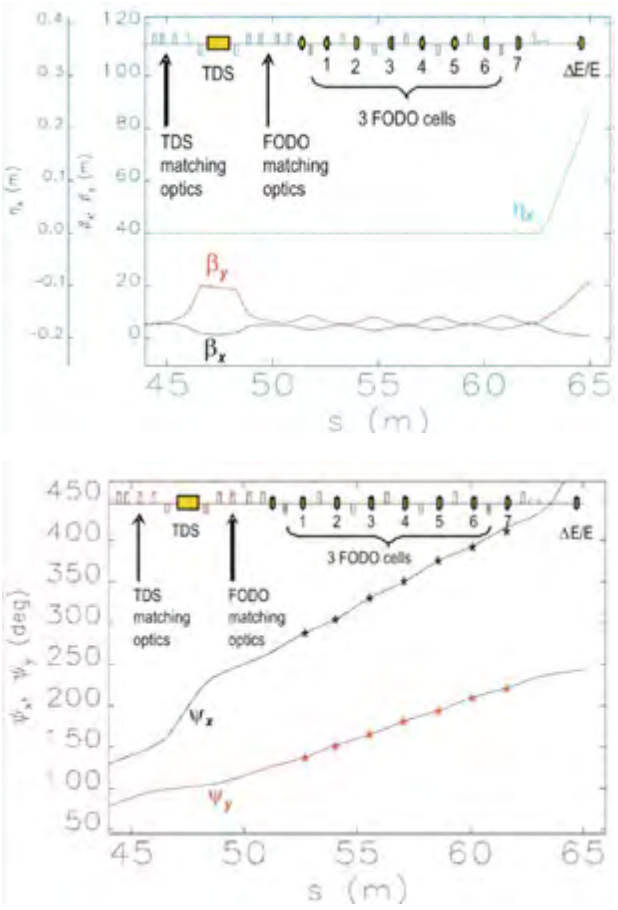

Figure 21: β-functions and dispersion (left side) as well as phase advances (right side) along the 250 MeV SwissFEL Test Injector diagnostics line.

A total of 8 BPMs will ensure sufficient beam trajectory control along the diagnostics section and a third ICT will be used for beam charge measurement and determination of overall transmission through the 250 MeV injector. As already indicated in the previous paragraph, an EO bunch length monitor applying the technique of spectral decoding (≤150 fs time resolution at 200 pC bunch charge) will be installed behind the bunch compressor for online monitoring of the longitudinal bunch charge

distribution. Although, this device provides redundant information compared to the TDS for the case of the 250 MeV test injector, it is foreseen to simplify the design and to improve its robustness for online operation in the background in order to provide a non-destructive, single-bunch longitudinal profile measurements behind the 1st bunch compressor of SwissFEL for its 200 pC operation mode.

4.4.5 Summary of the proposed Electron Beam Diagnostics

A summary of the diagnostics components is given in Table 10 through 12. It follows the previously introduced partition of diagnostics sections in a low energy branch, the linac segments and a high energy branch.

Device Name	# of Devices	Measured Property	Resolution
Button beam position monitor	1	Beam position	$\sigma_{avg}/5$ (100 µm)
Res. stripline beam position monitor	1	Beam position	10 µm @10–200 pC
Optical screen monitor (OSM)	4	Beam profile/position Energy /energy spread	~10 µm ~10^{-4}
“Pepperpot” / slits	1	Emittance	<100 nm rad
Integrating current transformer (ICT	1	Charge, transmission	<5 pC (<1 pC)
Faraday cup (FC)	1	Time structure/charge	<200 ps / 10%
Wall current monitor (WCM)	1	Time structure/charge	<200 ps / 10%
Bunch length monitor (BCM)	1	Bunch length using Electro Optical Sampling	>500 fs (over 20 ps)
Bunch arrival time monitor (BAM)	1	Arrival time using EO-detection, based on optical timing and synchronization	<10 fs
Deflecting cavity	1	Longitudinal current profile and slice parameters	<200 fs

Table 10 low energy (8 MeV) diagnostics devices.

Device Name	# of Devices	Measured Property	Resolution
Beam position monitor (BPM)	3	Beam position	10 µm @10–200 pC
Optical screen monitor (OSM)	3	Beam profile/position	~10 µm

Table 11: diagnostics devices in between the linac accelerator structures.

Device Name	# of Devices	Measured Property	Resolution
Stripline beam position monitor (BPM)	15	Beam position	10 µm @10–200 pC
Optical screen monitor (OSM)	15+5	Beam profile/position	~10 µm
Synchrotron radiation monitor (SRM)	1	Beam profile/position Energy spread	~10 µm ~10^{-4}
Integrating current transformer (ICT	2	Charge, transmission	<5 pC (<1 pC)
Bunch arrival time monitor (BAM)	1	Bunch arrival time	<10 fs
EO bunch length monitor (BLM)	1	Bunch length	~150 fs
Bunching monitor (BM)	1	Bunching using coherent FIR radiation	relative measurement
Transverse RF deflecting cavity	1	Sliced beam properties and bunch length	~20 fs (200 pC) ~10 fs (10 pC)

Table 12: high energy (250 MeV) BC and diagnostics section devices.

4.5 Laser system

A copper photo-cathode is presently the base line electron source candidate fulfilling the SwissFEL injector requirements in terms of beam brightness. For the commissioning of the 250 MeV injector a laser system capable of generating 200 pC of photo-electrons is required. A minimum energy per pulse of 100 µJ at 266 nm is required to produce 200 pC of photoelectrons from a copper surface assuming a QE of 10^{-5}. Such pulse energies can be achieved with presently available Ti:Sa amplifier systems. In addition, Ti:Sa laser systems provide pulses as short as 100 fs so that it becomes possible to generate a uniform longitudinal profile (square profile) with a rise time of few 100 fs by frequency domain pulse shaping. The design, installation and operation of such laser system are not trivial. A collaboration with the Laser Group of the University of Bern has been initiated for UV pulse characterization techniques [41].

The emitted bunch charge distribution is almost a direct image of the longitudinal and transverse profile of the laser pulse. The influence of the laser shape on emittance preservation is well known. Some ideal profiles known as “waterbag” profiles would ultimately linearize the intra-bunch space charge forces [42] so that emittance compensation scheme would be applicable. Development of novel laser pulse shaping techniques will be done in collaboration with a French company (Fastlite).

A Ti:sapphire based amplifier system with subsequent frequency conversion stages is the most promising starting point for R&D activities to reach the required gun laser performance (Table 13). Ti:sapphire systems are commercially available and have reached a high technological maturity due to their widespread use in research laboratories throughout the world. In addition, many diagnostics tools and pulse shaping techniques are available for the near-IR/visible spectral region and frequency-tripling of the fundamental laser wavelength allows easy access to the UV.

Conventional Ti:sapphire amplifiers, however, suffer from spectral narrowing due to the limited gain bandwidth yielding spectra of 30–40 nm (FWHM) at the mJ level making wavelength tuning impossible. The scheme presented here has the potential to overcome this limitation and offers in addition enhanced pulse energy stability and direct UV pulse shaping. This should help to produce electron bunches with lower emittance at the gun.

Laser specifications	
pulse energy	200 µJ
central wavelength	250–300 nm
bandwidth	2-3 nm
pulse repetition rate	100 Hz
laser spot size on cathode (s)	0.1–0.27 mm
pulse rise time	<0.7 ps
pulse duration (FWHM)	3–10 ps
longitudinal pulse form	various
transverse pulse form	Uniform
laser to RF phase jitter	<100 fs
UV pulse energy fluctuation	<0.5 % rms
pointing stability on cathode	<1 % ptp

Table 13: Gun laser characteristics for SwissFEL.

4.5.1 General Layout

The laser system (Figure 22) consists of 4 subsequent amplifier stages. As seed laser, a Rainbow oscillator (Femtolaser, Inc.) delivering 380 mW is used, pumped by a 5 W Verdi (Coherent, Inc.). To improve the long-term performance of the oscillator a beam pointing stabilizer has been installed on the pump beam consisting of a 4-quadrant photodiode and a piezo-driven mirror mount.

The pre-amplified (10µJ) and temporally stretched (≈200 ps) pulse seeds the regenerative amplifier. An acousto-optic programmable gain control filter (Mazzler, Fastlite Inc. [43]) is situated in the regenerative cavity and is used as an adaptive spectral filter to counteract spectral narrowing during amplification. Broad spectra of up to 100 nm (FWHM) are subsequently amplified in two sequential multi-pass amplifiers and finally compressed to 20 fs, 18 mJ. Six identical Q-switched, frequency-doubled Nd:YAG pump lasers (Centurion, Quantel, Inc.) have been chosen to pump the various amplifier stages with a total pump power of 120 mJ.

The compressed pulses are frequency-converted from the near-IR to the UV by second harmonic generation (SHG) in a β-barium borate (BBO) crystal (type I, 0.5 mm, φ=29.2°, ϕ=90°) and subsequent sum-frequency generation (SFG) in a second BBO crystal (type I, 0.5 mm, φ=42°, ϕ=90°). The fundamental temporal pulse shape is optimized for highest UV conversion efficiency by the grating based compressor and a Dazzler located after the pre-amplifier. At this point the Dazzler is used to

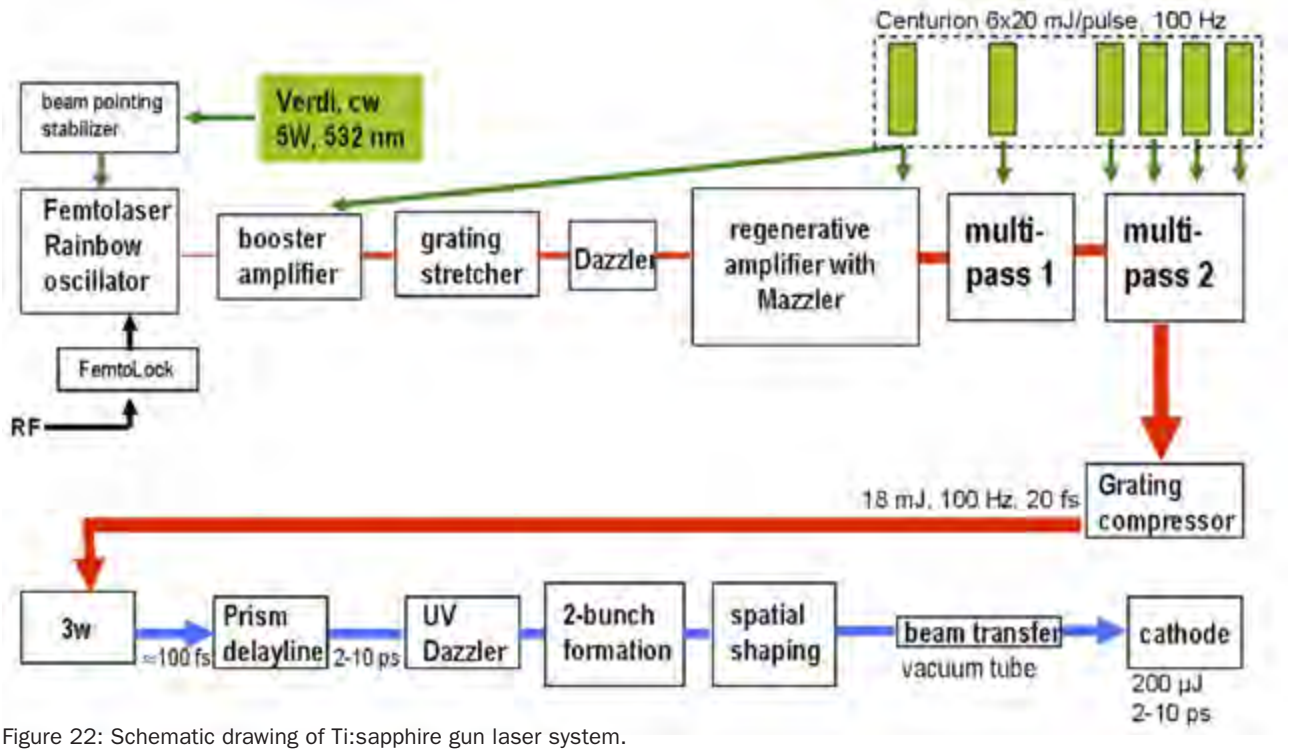

Figure 22: Schematic drawing of Ti:sapphire gun laser system.

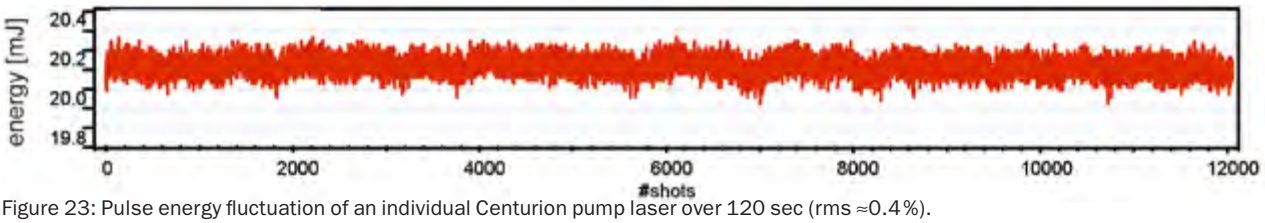

Figure 23: Pulse energy fluctuation of an individual Centurion pump laser over 120 sec (rms ≈0.4 %).

compensate for third-order dispersion to avoid detrimental satellite pulses.

Temporal pulse forming will be done by a low-loss prism-based pulse stretcher followed by an acousto-optical programmable dispersive filter (UV-Dazzler, Fastlite Inc.) while transverse homogenization will be realized by selecting the core part of the intensity profile by a spatial mask [44] which is relay-imaged onto the cathode surface.

4.5.2 Pump laser cluster

Each of the Centurion pump lasers provides 20 mJ @532 nm at a repetition rate of 100 Hz. The large number of six identical pump lasers is uncommon for the performance of the presented amplifier system. In principle one single powerful pump laser could provide the required pump energy. The present design, however, has been a consequence of stability constraints of existing commercial amplifier systems. To fulfill the stringent stability requirements of the gun laser we have chosen the following approach. First, compact diode-pumped Q-switched lasers (Centurion) from Quantel [45] have been chosen since they provide lowest rms energy fluctuations (<0.4 % rms) at 532 nm (Figure 23).

Second, to increase stability further the number of pump lasers have been increased to six since pump-laser induced energy fluctuations can be significantly reduced by mixing different pump sources. In principle, the net noise of N pump lasers will be decreased by a factor of $\sqrt{N}$ compared to a pump laser providing the same amount of pump energy. The employment of six pump lasers reduces the noise floor by a factor of ≈2.5. Preliminary measurements show, that the rms stability of the amplified pulse (0.34 % rms) is in fact better than the performance of one individual pump laser (0.4 % rms) (Table 14).

4.5.3 Wavelength selection

Control of the central laser wavelength (i.e. the laser photon energy) is helpful to produce low-emittance electrons [46]. Electrons leaving the metal surface by photoemission have a kinetic energy $E_{kin} = h\nu - \phi_{eff}$, and thus a thermal emittance $\varepsilon_{th} \propto E_{kin}^{1/2}$ arising from the mismatch of the photon energy hν and the cathode work function ϕ_{eff}. The total emittance may be reduced by adapting the laser photon energy to the net work function of the cathode material.

Despite the large gain curve of Ti:sapphire crystals (600–1100 nm) conventional amplifier systems provide spectra of only 30–40 nm centred around 800 nm due to gain narrowing effects. In our system an acousto-optical gain shaper (Mazzler) implemented in the regenerative amplifier helps to overcome such bandwidth-limiting effects [47].

The Mazzler introduces a wavelength dependent loss inversely to the Ti:sapphire gain curve in order to achieve a flattening of the net gain over a large spectral range. The resulting flat-top like spectrum reaches typically ≥80 nm bandwidth at FWHM (Figure 24). For pulse shaping purpose, however, spectra of 15–25 nm (FWHM) at the fundamental wavelength provide enough bandwidth for the generation of flat-top UV pulses with a rise time of <0.5 ps.

Wavelength selection is performed by the Dazzler. The current amplifier scheme allows continuous variation of the central wavelength within a range of 760 to 840 nm with a spectral width of 25 nm (Figure 25). Pulse energy and pulse stability (rms/peak-to-peak) of individual spectral slices are independent of the central wavelength as depicted in Table 14.

λ central (nm)	785	805	835	805
bandwidth (nm)	25	25	25	90
stability (%, rms)	0.39	0.36	0.39	0.35
stability (%, P2P)	2.2	2	1.7	2.8
duration (min)	2	2	2	2
pulse energy (mJ)	18.2	18	17.9	18.2

Table 14: Ti:sapphire stability for individual spectral slices.

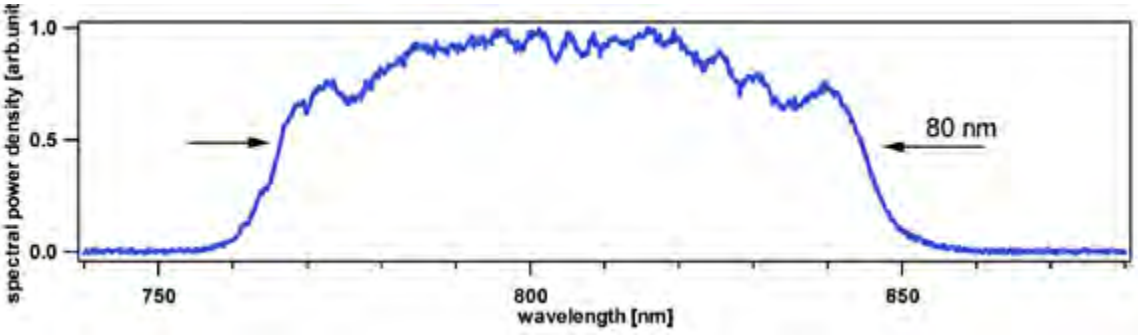

Figure 24: Broadband amplification in Ti:sapphire thanks to acousto-optical gain control.

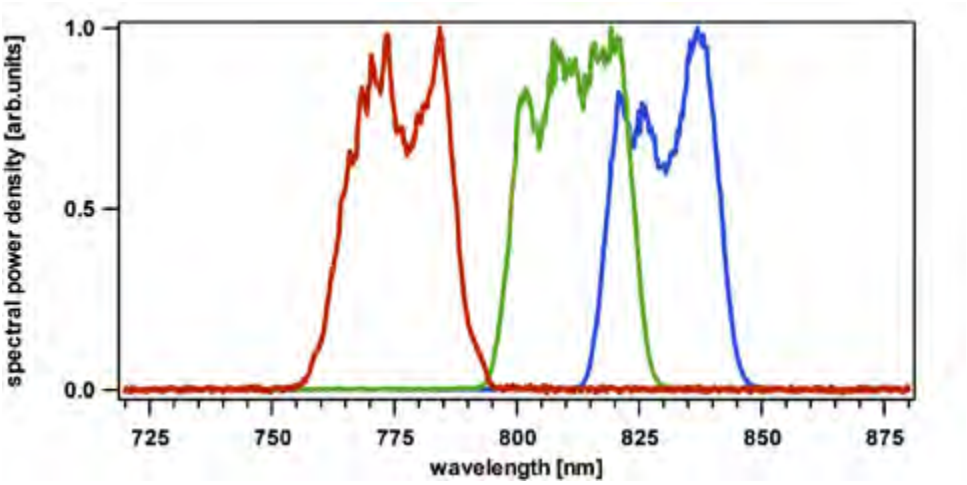

Figure 25: Wavelength-selected narrow-band amplification.

4.5.4 UV pulse shaping

The spatial and temporal shape of the amplified laser pulse is nominally Gaussian. Electron beam dynamics simulations indicate, that a flat-top like pulse shape helps to generate uniform temporal and spatial electron distribution resulting in a lower transverse emittance at the gun. Since other simulations show that a Gaussian-like electron distribution is less sensitive to timing jitter in the undulator it is more likely that an intermediate pulse shape will be optimal for best FEL performance [48]. Therefore powerful pulse shaping tools are required.

The formation of arbitrary UV pulses, however, has been non trivial. In the past indirect techniques have been applied such as frequency-domain pulse shaping at the fundamental wavelength (near IR) due to the lack of appropriate shaping tools in the UV. The required conversion process to the UV, however, can lead to strong distortion of the original pulse shape due to the nonlinearity of the process.

Our approach for achieving high-quality arbitrarily shaped UV pulses is based on direct UV pulse stretching and shaping. This became possible very recently thanks to the availability of an efficient acousto-optical pulse shaper working in the UV (UV-Dazzler, Fastlite Inc.). This device allows efficient phase-and amplitude control in the wavelength range of 250–400 nm. With a resolution of 0.1 nm and a deflection efficiency of up to 40 % at 250 nm the UV Dazzler should allow the formation of powerful arbitrarily shaped UV pulses. To avoid intensity-induced nonlinear absorption in the KDP crystal the UV Dazzler is seeded with UV pulses stretched to several ps. For temporal pulse stretching we designed a dedicated prism assembly shown in Figure 26.

Figure 26: UV pulse stretcher based on a double-prism sequence.

Efficient pulse stretching in the UV is challenging since gratings, which are commonly used for pulse stretchers in the near-IR, suffer from high losses in this wavelength range. In fact, the expected energy throughput of a grating-based stretcher would be <20 %. A prism-based design seems more promising. Various glass substrates from different suppliers have been tested at PSI in order to optimize the energy throughput by minimizing intensity-induced two-photon absorption but still offering a large angular dispersion to keep the geometrical dimensions of the stretcher small.

A prototype double-prism stretcher is currently being built at PSI based on Corning 7980 HPFS glass substrates. Ray-tracing calculations indicate that a distance of 3 m is required to stretch the UV pulse from ≈100 fs to the required 9.9 ps. The expected energy throughput should be close to 80 %. The pulse length can be continuously varied within 2–9.9 ps by adapting the geometrical distance between the two prism pairs.

We expect the UV-Dazzler / UV-stretcher combination to be a powerful tool for arbitrarily temporal pulse shaping providing the requested UV pulse quality. Temporal pulse characterization will be performed by cross-correlation with the fundamental laser pulse.

4.5.5 Laser-Room for the SwissFEL Injector

The amplitude stability of laser systems is highly dependent on environmental conditions (temperature, air turbulence, humidity). In order to provide the best environmental quality for the laser system, the SwissFEL injector will include a temperature and humidity controlled clean room. The room provides a Class 10000 environment with a temperature stability of ±0.1°C. The humidity is limited to a maximum of 50 % in order to avoid condensation on warm optical components.

The analog and optical Master Oscillator also require a stable environment. For this reason both will be in the laser room.

4.6 Girder system and alignment concept

For the girder design we decided to take profit of the experience accumulated with the SLS girder system. The component positioning and alignment concept is based on the SLS design [49, 50] while the girder material will be mineral cast. For the alignment two rails machined and polished with a precision of 100 µm over 4.7 m will define the reference surface for a direct positioning of all components (Figure 27). Fine adjustment of the components on a given girder will be performed using calibrated thickness blocks (shimming), the relative position girder to girder will be adjusted using the girder jacks.

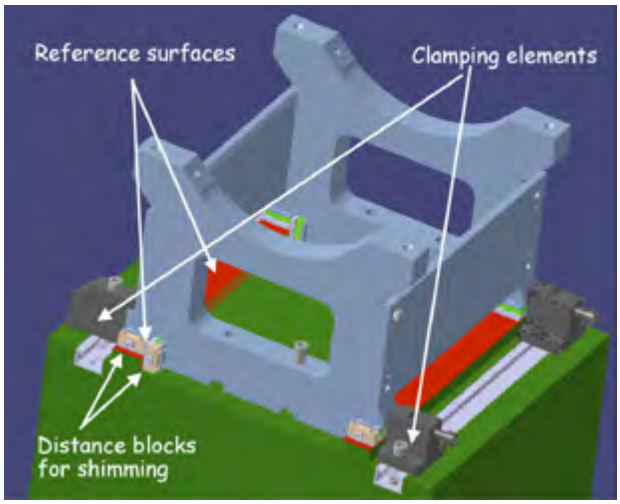

Figure 27: Support system for the S-band cavity solenoids. In green a section of the girder, in red the polished reference surfaces.

The basic design criteria are summarized in Table 15.

Eigenfrequency >50 Hz
High internal damping
Each component can be adjusted individually with minimum increments <50 µm
Universal generic alignment concept for all components
Repeatability of adjustments <0.01 mm for critical components
Easy to adjust the level of the girder after settling of the ground floor (without changing the horizontal position)
Cost efficient for SwissFEL
Pre-assembly of components on girders
Mechanical accuracy of components in relation to the girder, without adjustments, better than 0.1 mm

Table 15: Design criteria for the Girder system.

To achieve the required stability and to optimize the cost the option of using mineral cast will be investigated in the 250 MeV injector facility. This material has properties very close to granite and is relatively widely used to manufacture stable support tables for precision machining tools. Until now it has never been systematically studied for girder systems supporting accelerator components.

The main advantages of mineral cast can be summarized has:

- high damping properties expected, non homogenous material
- high eigenfrequency as one solid block
- cost effective in mass production (no high temperature processes)
  - one wooden mould gives ~10 girders
  - one steel mould gives +100 girders
- surfaces can be ground to precision of 0.1 mm over the length
- no local stresses introduces by machining

To avoid strong coupling with the ground motion particular care has to be taken to push the first resonant modes above 50 Hz where the energy transfer from the ground to the structure become less efficient and the absolute ground displacements smaller. Table 16 shows typical eigen-frequencies of such a girder.

Modus	Frequency [Hz]	
1	116.89	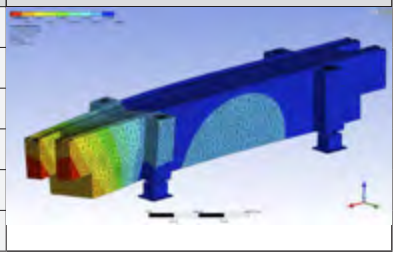
2	125.16	
3	147.5	
4	179.6	
5	212.16	
6	231.62	

Table 16: Simulated resonant frequency for a mineral cast girder. The picture illustrate the first vibration mode of the mineral cast girder.

5 Beam dynamics simulated performances

5.1 Initial conditions

For a realistic simulation and optimization of the electron source it is necessary to evaluate the uncorrelated intrinsic emittance at the emission from the cathode surface. For photo emission this value depends on the difference between the laser photon energy and the effective potential barrier in the crystal bulk in the presence of an external electric field (Figure 28).

The assumptions on the initial intrinsic emittance are based on the measurements performed recently with photo cathodes at PSI [51] and SLAC [12]. The summary of these measurements are shown in Figure 29. For the simulations presented here below we considered a mean value between the intrinsic emittance measured at PSI and with the LCLS gun. Since the intrinsic emittance is the ultimate factor limiting the brightness of an electron source it is important to have a deep understanding of the emission process and to clarify the discrepancies between theory and measurements. A recent analysis of the photo-emission process from metal cathodes can be found in [52].

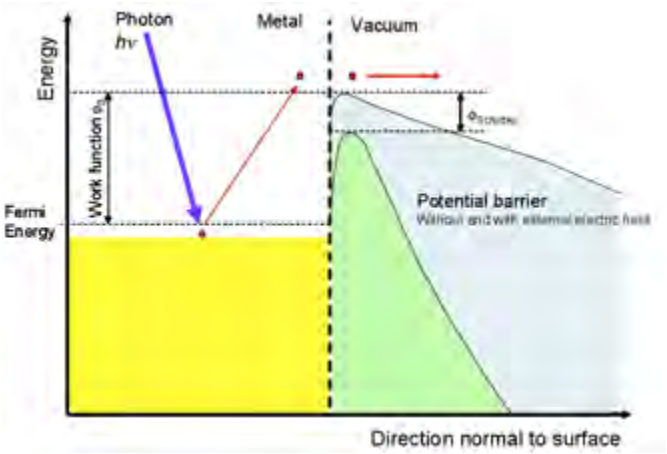

$$\varepsilon_{th} \approx \sigma_{x,y}\sqrt{\frac{h\nu - \phi_0 + \phi_{Schottky}}{3m_e c^2}} = \sigma_{x,y}\sqrt{\frac{2K_{av}}{3m_e c^2}} \quad (5\text{-}1)$$

$$\phi_{Schottky}(eV) \approx 3.7947 x 10^{-5}\sqrt{E(V/m)}$$

$$k_{av} = \frac{1}{2}(h\nu - \phi_0 + \phi_{Schottky})$$

Figure 28: Three step emission model and expression for the approximated intrinsic emittance.

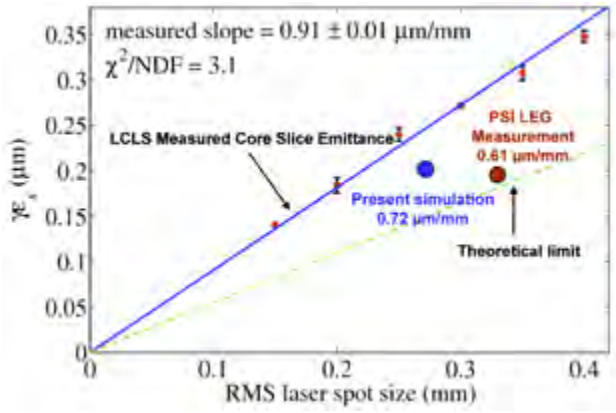

Figure 29: intrinsic emittance measurements performed with the LCLS RF photo injector (courtesy of D. Dowell) and at the PSI LEG test facility with a diamond turned copper cathode. The dotted line represents the theoretical value calculated by D. Dowell assuming a perfectly flat cathode surface. The blue dot is the value used for the simulation reported here below.

Note that the theoretical evaluation of the intrinsic emittance discussed above doesn't take into account the quality of the cathode surface; In particular the surface roughness can deteriorate sensibly the thermal emittance and could explain the discrepancy between the measured values and the theoretical ones. In the CTF3 gun the cathode can be relatively easy exchanged allowing studies with respect to the cathode preparation procedures.

Parameter	200 pC	10 pC
K_{av} (eV)	0.4	0.4
Intrinsic Emittance (mm.mrad)	0.195	0.072
Laser rms Size (μm)	270	100
Laser Rectangular Pulse FWHM (ps)	9.9	3.7
Laser Rise and fall Time (ps)	0.7	0.7
Peak Current (A)	22	3
RF peak gradient (MV/m)	100	100

Table 17: Beam parameters at the photo cathode for high and low charge operation.

The initial beam parameters are summarized in Table 17. As discussed above, a smaller intrinsic emittance can be obtained by decreasing the laser spot size at the cathode. However for a given charge the dilution effects due to longitudinal and transverse space charge restrict our degree of freedom. Therefore the peak current and gradient in the gun must be globally considered while optimizing the laser spot size and pulse length. The laser rise and fall time correspond to the new Titanium-Sapphire laser system described in the paragraph 4.5.

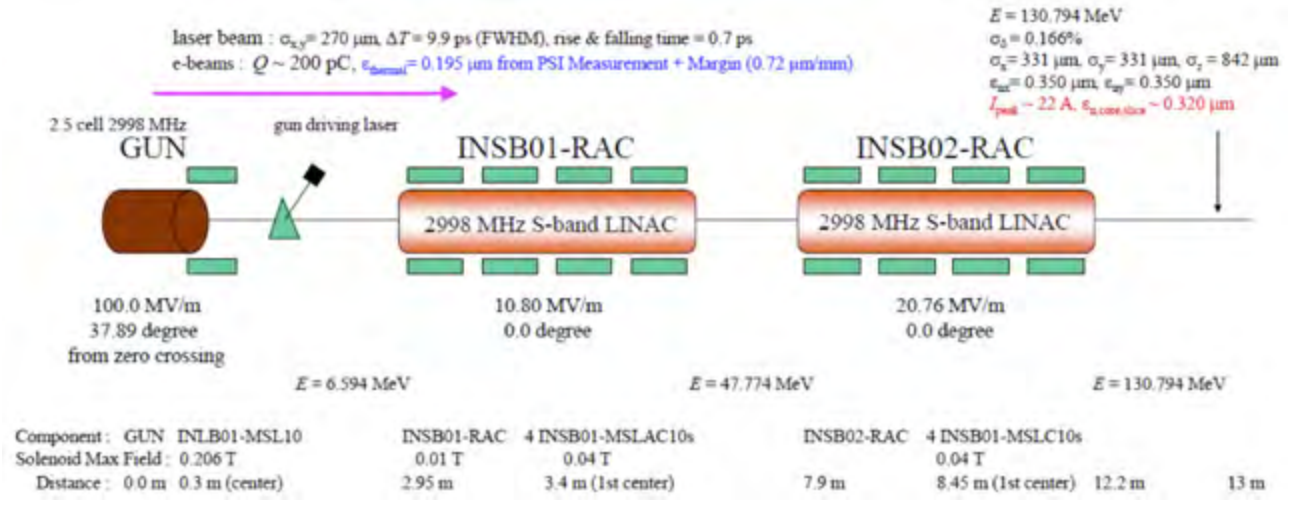

Figure 30: Summary of the optimized parameters for 200 pC operation and 100 MV/m at the cathode.

5.2 Injector optimizations

5.2.1 Invariant envelope matching

The injector start to end simulations have been described in [53]. Since the FEL interaction is a local process restricted to a co-operation length, only the electron bunch slice parameters determine the FEL radiation properties. Nevertheless for optimal performance of the facility it is important to guarantee an optimal Twiss parameter matching along the electron bunch and consequently a good compensation of the projected emittance from the beginning of the accelerator. To achieve this result the beam is manipulated at low energy benefiting from the emittance fluctuations induced by the space charge according to the technique known as "invariant envelope matching" [54, 55]. For this purpose a solenoid magnet is placed just at the exit of the RF photoinjector to refocus the beam in front of the first travelling wave accelerating structure. The exact positioning of the first accelerating structure must be optimized and depends mainly on the charge density and beam energy (for the geometry see also Figure 20).

In the configuration studied here the invariant envelope matching is practically completed after the first two accelerating structures where the beam parameters are frozen by the high energy. Figure 30 illustrates the typical parameters of the gun and the first two travelling wave cavities for optimum operation with 200 pC and 100 MV/m at CTF3 gun cathode.

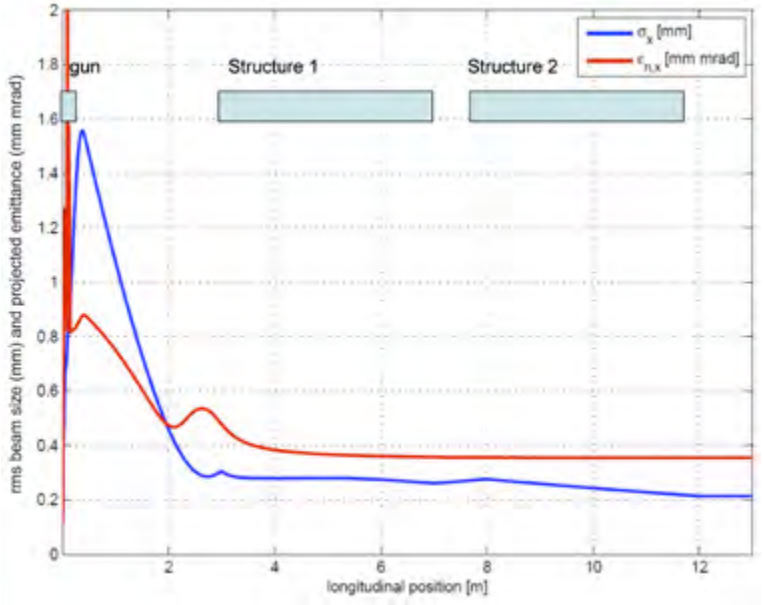

Figure 31: Normalized emittance and beam envelope along the first 12 m of the injector.

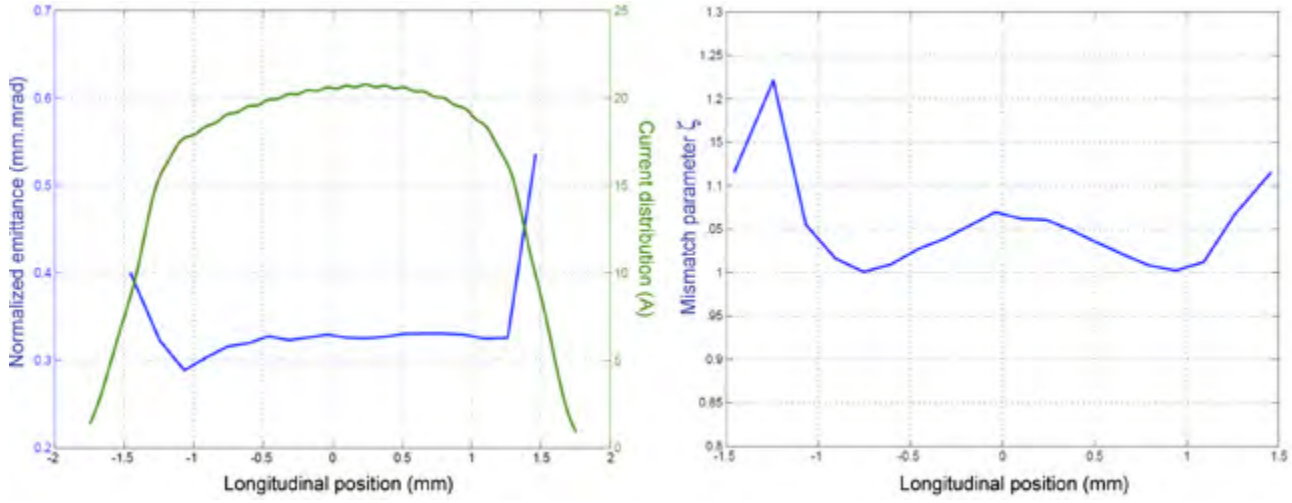

Figure 32: Current profile and slice emittance (left) and mismatch parameter (right) at 130 MeV after two travelling wave accelerating structures.

Figure 31 illustrates the evolution of the projected normalized emittance and beam envelope up to 130 MeV for the situation illustrated in Figure 30. The first accelerating cavity is positioned 2.95 m from the cathode at the optimum matching point.

The quality of the matching can be measured looking at the slice emittance along the bunch and using the beam mismatch parameter given by:

$$\zeta = \frac{1}{2}(\beta_0\gamma - 2\alpha_0\alpha + \gamma_0\beta) \qquad (5\text{-}2)$$

Where β_0, α_0, $\gamma 0$ are the matched projected Twiss parameters and β, α, γ the slice Twiss parameters. If the mismatch parameter is equal to 1 all slices have the same Twiss parameters and the matching is perfect. In general after emittance compensation in the injector the mismatch parameter for the beam core should be kept below 1.1. Figure 32 shows the mismatch parameter and slice emittance at 130 MeV for the optimized configuration described here above.

After fixing the relative position between cathode and first accelerating structure for the nominal operation the optimization procedure can be applied for different charges. Table 18 shows a summary of the simulation results for charges between 200 and 10 pC at 130 MeV.

Charge (pC)	Laser pulse FWHM (ps)	$I_{peak,\ cathode}$ (A)	Laser $\sigma_{x,y}$ (µm	$\varepsilon_{intrinsic}$ (µm. rad)	$\varepsilon_{slice}/\varepsilon_{projected}$ (µm.rad)
200	**9.9**	**22**	**270**	**0.195**	**0.320/0.350**
150	9.0	18	245	0.177	0.272/0.283
100	7.9	14	214	0.155	0.220/0.233
50	6.2	8.7	170	0.123	0.160/0.174
20	4.6	4.7	125	0.091	0.108/0.122
10	**3.7**	**3**	**100**	**0.072**	**0.080/0.096**

Table 18: Optimized parameters for different charges between 200 and 10 pC.

Note that the invariant envelope matching is relatively insensitive to RF phase variations in the photo-injector, while a significant modification of the matching conditions can be observed when changing the gun gradient and the solenoid focusing field of 1%. Figure 33 shows the expected performance deteriorations if one modifies the above mentioned parameters around the optimum settings for the operation with 100 pC.

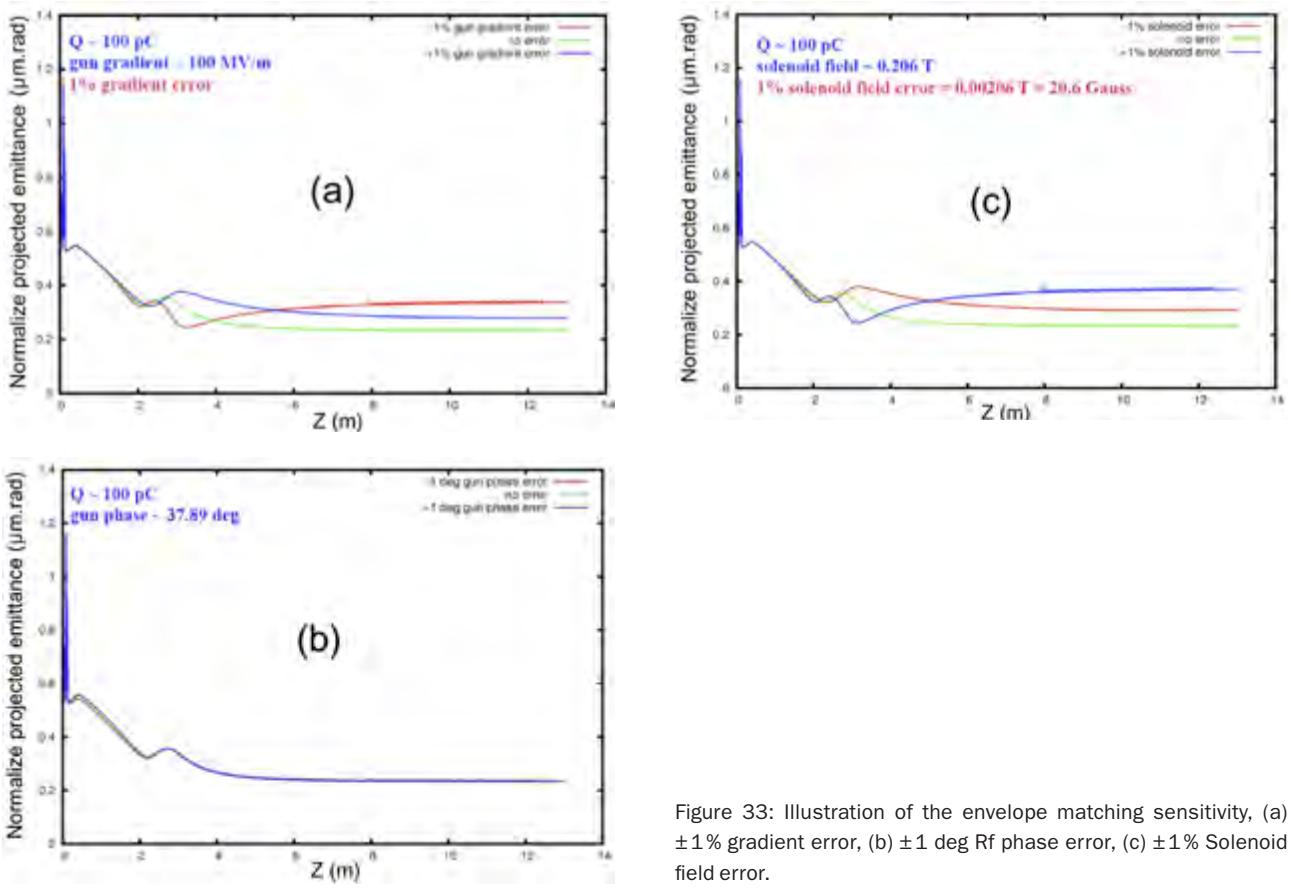

Figure 33: Illustration of the envelope matching sensitivity, (a) ±1% gradient error, (b) ±1 deg Rf phase error, (c) ±1% Solenoid field error.

5.2.2 Overall Injector optimization

A schematic layout of the overall injector including a possible upgrade with an undulator line is shown in Figure 34. After performing the invariant envelope matching the electrons are accelerated off crest in the S-band traveling wave cavities up to ~275 MeV. This process induces the necessary energy correlation along the bunch for the longitudinal compression in the magnetic bunch compression chicane (BC). In front of the BC an 12 GHz X-band cavity operated in deceleration mode is used to remove the longitudinal non linearity introduced by the RF during the previous acceleration stages.

The lattice and optic in the bunch compressor region has been optimized to minimize the emittance growth

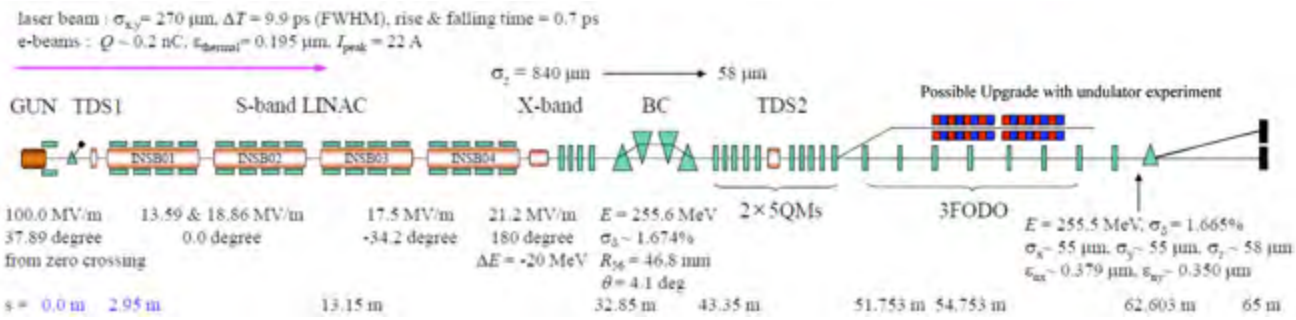

Figure 34: Full injector facility - optimization for 200 pC operation.

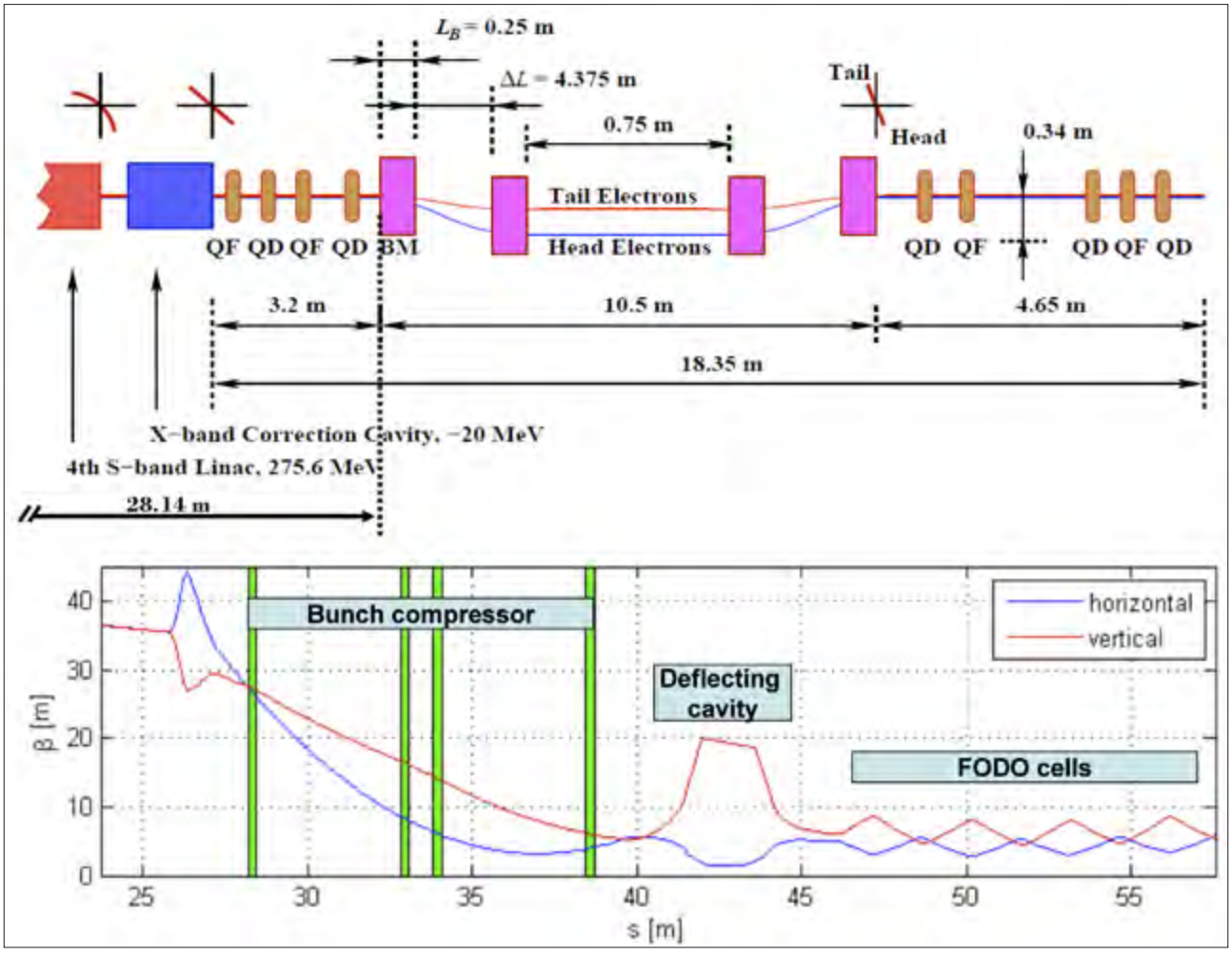

Figure 35: Compression chicane layout and optics from the compression chicane to the FODO cells.

due to CSR effects in the dipoles, while the optic in the diagnostic section has been optimized to allow quick switches from projected and slice parameters measurements without adjustments of the transport line. Figure 35 shows the concept of the compression chicane and the nominal optics. The transversal position of the central dipoles will be adjustable to have maximum flexibility for the compression studies.

Since the large dispersion in the center of the BC induces a transverse beam size of σ_x~5.5 mm the dipole magnets must be designed with a large "good field" region to avoid non linear dispersion and non linear focusing effects that could dilute the emittance after compression [56]. The design retained for the injector dipoles has been optimized using the 3D solver TOSCA [57]. As shown on Figure 36 the expected relative deviation in integrated field at different transverse positions defines a "good field" region with $\Delta B_{integrated}/B < 5 \times 10^{-5}$ extending over ±40 mm.

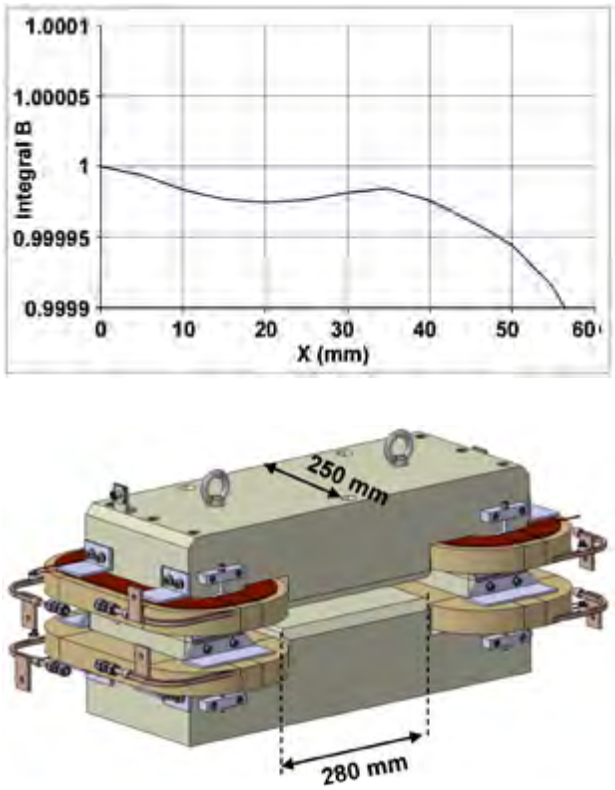

Figure 36: Compression chicane dipole, design for large "good field" region.

Table 19 summarizes the expected beam characteristics after compression. According to these simulations the injector should deliver a beam fulfilling the SwissFEL requirements. For the final SwissFEL injector we are currently studying an increase of the injector energy up to a maximum of 450 MeV to alleviate space charge effects during compression.

Parameter	200 pC	10 pC
Energy (MeV)	255	
Rms Bunch Length (fs)	193	33.2
Rms Projected Emittance (mm.mrad)	0.38	0.1
Rms Slice Emittance (mm.mrad)	0.33	0.078
Peak Current (A)	352	104

Table 19: Beam parameters after compression for high and low charge operation.

6 Commissioning and operation program

The machine commissioning will consist of three main phases. For all these phases the repetition rate in operation with beam is limited to **10 Hz**. In special test modes the RF plants could be operated at 100 Hz with the exception of the RF-gun (CTF3 gun #5) which is limited to maximum 10 Hz and the deflecting cavities limited to 50 Hz.

6.1 Definition of the main commissioning phases

Phase 1 is dedicated to the commissioning of the RF photoinjector and the first 3 m transport line, downstream some additional screens are added for beam diagnosis . The component assembly and the infrastructure preparation must allow early operation of the gun while assembling the rest of the machine. For this purpose the linac tunnel will be divided in two sections by a movable concrete wall shielding the area downstream of the gun region. Inside the gun bunker it is foreseen to start, parallel to the gun commissioning, the early conditioning of the travelling wave structures. Commissioning of phase 1 will start with a Nd:YAG laser while awaiting for the commissioning and optimization of the more sophisticated Ti:Sa laser system. The Nd:YAG laser will allow full commissioning of all components and procedures, with the exception of invariant envelope matching, which relies on the longitudinal charge distribution provided by the Ti:Sapph laser.

For phase 2 the machine will be fully assembled with the exception of the X-band harmonic cavity and the bunch compressor. The beam will be accelerated down to the diagnostic straight first without compression and invariant envelope matching optimized for smallest emittance. The machine and the measurements procedures will be optimized avoiding the additional complications due to the small aperture and high impedance of the harmonic cavity.

The X-band cavity is required for phase 3 to perform systematic studies of the bunch compressor. In order to reach the high peak current at the undulator a two stage compression is foreseen for SwissFEL. The first, stronger, compression stage happens at the end of the injector linac via a magnetic compression chicane. The coherent and incoherent synchrotron radiation emitted by the electron along the chicane dipoles and collective effects like micro-bunching instability can seriously dilute the beam emittance if not kept under control. The verification of the beam parameters as reported in Table 19 are the main goal of the beam dynamics scientific program at this phase of the commissioning.

Main steps phase 1:

- RF conditioning CTF gun up to 100 MV/m
- Laser alignment on cathode (laser pointing stability, laser-RF synchronization)
- Beam-based alignment of gun solenoid
- Schottky-scan to find laser reference phase, cathode wquantum efficiency
- Dark current characterization
- Beam-based alignment of magnets

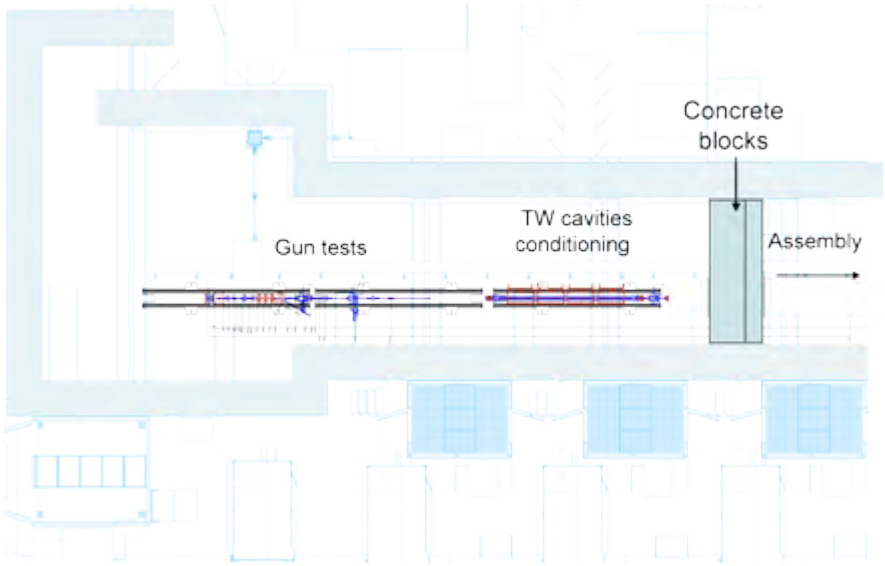

Figure 37: Location of the temporary shield inside the tunnel.

- Commissioning of the spectrometer: momentum and momentum spread (RF phase scan)
- Commissioning BPMs: beam orbit and stability
- Beam envelope and projected emittance (slits)
- Invariant envelope matching (Ti:Sapph laser)

Main steps phase 2:
- Complete RF conditioning S-band structures
- Beam-based alignment of magnets and RF structures
- Commissioning BPMs: beam orbit and stability
- Commissioning of transverse deflecting structures: bunch length and slice emittance
- Optics-based measurement of projected emittance
- Invariant envelope matching for minimum projected emittance at 250 MeV

Main steps phase 3:
- RF conditioning X-band structures
- Beam-based alignment of X-band structure
- Bunch compressor studies: compression vs. S- and X-band phase, deflection angle (R_{56})
- Micro-bunching and coherent optical transition radiation

6.2 Operating regimes

In addition to the commissioning phases dictated by the installation schedule, we define operating regimes in terms of bunch charge and beam energy. On the one hand this is required by radiation protection, such that radiation measurements can be performed every time a new operating regime is entered. On the other hand, a finite set of operating regimes facilitates comparisons between measurements as well as to simulation. The charge regimes are defined according to Table 2 as 10 pC (low charge), 100 pC (medium charge) and 200 pC (high charge). For the energy, there are just two regimes, low energy (gun only, up to 8 MeV), and high energy (full linac, up to 280 MeV).

6.3 Software applications and data storage

Closely linkt to commissioning is the development of software applications needed to perform the activities listed above. Here the aim is to provide a set of tools which will allow regular operators to execute the procedures and measurements needed to operate the machine.

While simple manipulations of device readings are handled within the low-level EPICS toolkit (see 7.1.2), more advanced data treatment, in particular image processing, is mainly done within the MATLAB computational framework. A library for image processing has been developed and is used by all applications based on screen images (e.g., emittance measurements). Images and other data related to specific measurements are stored in the Nexus file format, a common standard in the X-ray, neutron and muon community. Nexus itself is based on hdf5 (hierarchical data format 5).

7 Controls

The control system plays a central role in all large facilities. It provides the connection between hardware and the operators, it creates the environment that allows physicists to do their measurements, and it archives data to allow comparison with simulations retrospectively. Guidelines for the design of the control system are reliability, ease of use and expandability. Beyond the pure functionality, the maintainability of the whole system and the portability to new developments in computer science are basic requirements.

The hardware and software platforms, boot and archive services, configuration management and logistics developed for the other PSI accelerators shall be used as far as possible. The control system for the 250 MeV Injector will benefit from existing control systems equipment standards and know-how of the other PSI accelerators whenever possible. Many applications can be based on the experience gained with SLS (Swiss Light Source) and the LEG gun test facility. Developments needed for the SwissFEL are to be accomplished in a manner that meets the project schedule, budget, and performance needs, with consideration for knowledge transfer – internally and to the wider accelerator community.

7.1 Requirements

A wide range of user groups, like physicists and operators, will require information and support from the control system. Therefore, on one hand, the control system has to be designed to allow modularity and possibility of integration for new systems and programs to ensure support of physicists. On the other hand, the system should be as standardized and easy to use as possible to support operators that have to care for all PSI accelerators.

The 250 MeV Injector is foreseen to be used as the injector in the final SwissFEL accelerator. That means that the key concepts of the control system should take this into account. But at the same time, the 250 MeV Injector provides the possibility to develop, test, and optimize components for the use in the SwissFEL facility.

The control system shall be implemented in such a way that it can be incrementally expanded and upgraded as the project proceeds. The control system must be able to be extended to new hardware and software technology during the project phase and later.

The control system has to be laid out in a way that it will scale up to the final scope of the facility without compromising performance. This includes the capability to cope with a pulse repetition rate of 100 Hz, even if this may not be needed for the 250 MeV Injector. Handling issues that might be necessary only for the SwissFEL like pulse rate limiting, restricted data rates (to operator displays, for example), pulse identification and time stamping and so on shall be considered in the design.

7.2 Control System Structure and Architecture

EPICS

The Control System will use the EPICS (**E**xperimental **P**hysics and **I**ndustrial **C**ontrol **S**ystem) toolkit. EPICS has been successfully applied at PSI in the SLS and in several similar large projects around the world (for example LCLS at SLAC). Due to its collaborative nature, using EPICS enables us to take advantage of work done at other laboratories. Using a standard software toolkit will allow us to make best use of in-house know-how and to consolidate technical support services.

Industry is supplying equipment with EPICS support and there are companies that can be contracted to provide EPICS support and applications when appropriate. This is a considerable advantage over having to integrate non-standard applications into the control system.

The EPICS toolkit includes:

- Network based client server model implementing Channel Access as network protocol
- Distributed process variable (PV) database that contain a process image of the machine parameters
- EPICS extensions like Alarm Handler, Archiver and GUI builder (medm) already known by operators
- Available Channel Access interfaces to common programming languages (for example to C, C++, Java, Tcl/Tk, Matlab and many more)

The general layout of an EPICS system is shown in Figure 38. The consoles in the control rooms run EPICS client applications that connect over Ethernet network to the distributed EPICS servers (called **I**nput **O**utput **C**ontroller) which control the hardware. In addition central services like the archiver are running on dedicated servers located in a server room. In all of these computers, customized programs requested by physicists can be implemented and integrated into EPICS.

Software Maintenance and Distribution

One goal of the control system of the 250 MeV Injector is to establish processes for easy distribution and maintenance of software for the SwissFEL accelerator. The SwissFEL control system will be roughly five to ten times bigger in terms of the number of controls components needed. Therefore, automation should be introduced where ever possible.

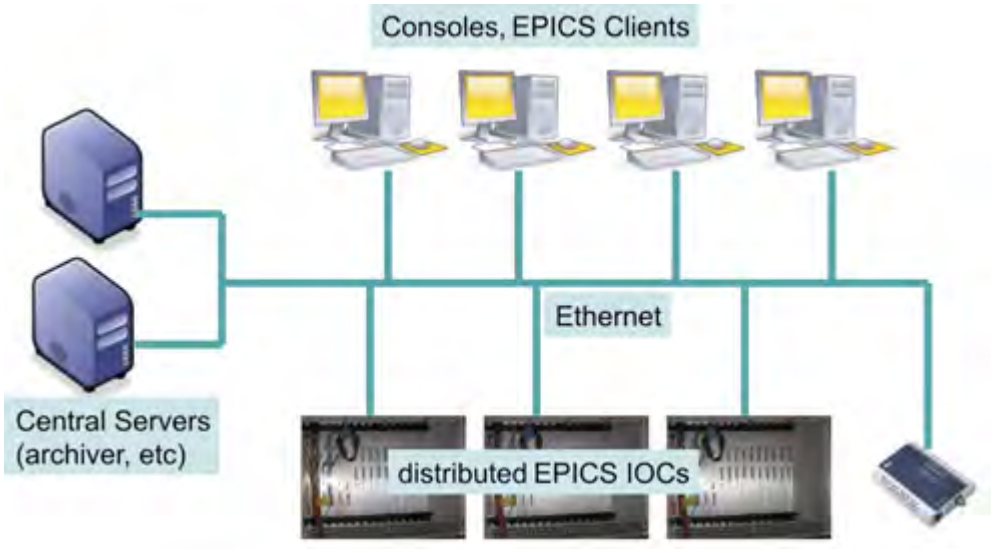

Figure 38: General EPICS system layout.

The general way of software distribution and installation is already established at the SLS. Further development might be needed to improve flexibility in order to integrate new hard- and software.

The basic information needed for the automated software installation is stored in relational databases. To make best use of in-house knowledge the environment provided by the IT department, namely Oracle databases, will be used.

Controls Hardware

For network components, file servers and PCs the 250 MeV Injector will use hardware based on PSI standards defined by IT department.

As far as reasonable possible hardware used at other PSI accelerators should be preferred to take advantage of existing expertise and cheaper stock keeping. Such hardware includes:

- VME crates and boards running the VxWorks Operating System (from Wind River): PSI has adopted the VME64x standard as its front-end hardware platform for the accelerator facilities. It shall also be used for the 250 MeV Injector. A rich set of modules like digital and analogue I/O as well as motor controller and encoder cards is supported.
- PLCs type Siemens S7: For autonomous subsystems and applications where high reliability is required but the speed requirements are lower, PLCs will be used. Typical applications are for example vacuum interlock, component protection systems and so on. The applications will be not be developed by the controls section, but have to be integrated into the control system for visualization and data archiving.
- motor driver stages developed at PSI
- digital power supply controller developed at PSI

Special requirements may be solved by using embedded controllers (for example FPGA-based or microcontrollers). Examples of such systems may include geographically isolated devices, systems that need the computing speed of a dedicated CPU, or entirely new hardware components which are not yet supported by any PSI standard hardware. However, the embedded controllers shall be integrated into the EPICS framework and the software maintenance and distribution processes.

Network Layout

The network layout of the 250 MeV Injector is especially designed in view of the SwissFEL requirements. There, the number of network ports needed is too high to fit into a class C subnet, which is standard at PSI. Therefore, the Injector will be used to develop, implement, and test the necessary procedures and programs to connect different subnets along the accelerator.

The planed network layout is schematically shown in Figure 39. Every circle in the sketch except "PSI Network" represents a class C network with 254 addresses. The connections of the different subnets of the EPICS network are controlled by Channel Access Gateways to minimize the network traffic. The control room is the central network to minimize the number of network borders for measurements and programs running in the control room.

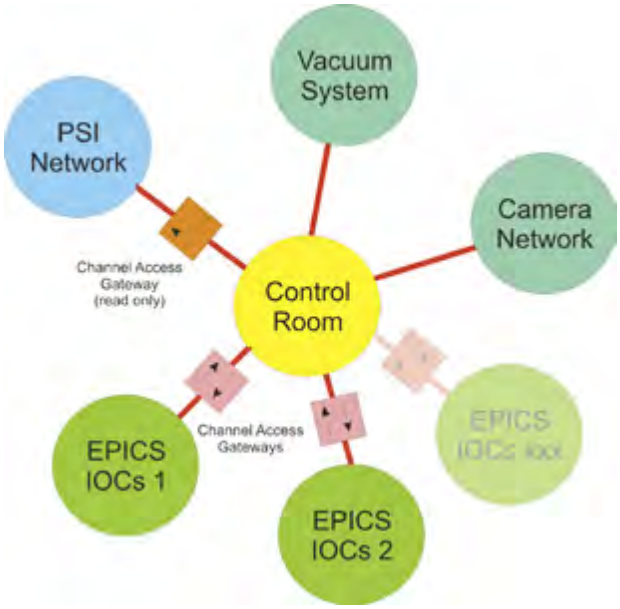

Figure 39: Planned Network layout.

7.3 Special Subsystems

Timing System

The timing system provides synchronized event distribution on a 10 ns time scale. This allows measurements and parameter settings to be triggered on defined time distances from each other. For example the beam current measurement can be triggered with a defined delay to the electron bunch creation at the gun.

Furthermore, the timing system provides a bunch number consisting of 52 bits. This allows for 252 bunch numbers ($4.5 \cdot 10^{15}$), which will be unambiguous over a period of time exceeding the lifetime of the SwissFEL at a repetition rate of 400 Hz.

The general functionality of the bunch numbering has already been tested at the gun test facility. Further tests will be done with the measurements planned in the injector to ensure easy usability of the system. The stable and reproducible synchronization of the gun laser and the RF phase will be an important point of investigation, especially in view of stable user operation at the SwissFEL.
The timing system is based on the SLS timing system which will be adapted and extended to the requirements of a linear accelerator with repetition rates up to 100 Hz. This might be needed only later in the SwissFEL accelerator but should be tested as far as reasonably possible in the 250 MeV Injector.

Interlock Systems
The interlock system could be divided into three main parts which differ in their speed requirements, complexity and protection goal:

1. PLC based Beam Loss Interlock System for radiation protection
2. Beam Permit System for equipment protection, based on the design of the Run Permit System used at the HIPA accelerator at PSI. This system is not needed for the 250 MeV Injector but is a test system for the Swiss FEL
3. Beam Quality Verification System as part of the EPICS environment, which will be designed and realized in the course of first experiences derived from the 250 MeV Injector

Only the first two described systems are safety relevant. They are independent of the EPICS environment in the sense that they could work without EPICS. EPICS can be used in these systems to visualize the situation and archive the data.

In addition (and not described here) there is the vacuum system with a dedicated interlock system that disables the electron gun in case of bad vacuum, the personal safety system (PSA) which is part of the radiation protection concept and local routines that supervise single components like RF structures.

8 Radiation Safety and Protection System

8.1 Introduction

For the SwissFEL injector test facility a new building [58] in the PSI-West-area is to be built in order to test the gun performance and beam line system, including a beam dump for electron energies up to 0.3 GeV. This document provides estimates of the radiation protection relevant parameters, such as the lateral shielding thickness and the beam dump dimensions and related shielding thicknesses, used as guideline for the civil engineer planning in 2009. The calculations are based on the "SHIELD11 computer code" that will first be shortly introduced.

8.2 The SHIELD11 computer code

The SHIELD11 code [59] has been developed at Stanford Linear Accelerator Center (SLAC) to perform shielding analyses in the vicinity of a high energy electron accelerator. It uses analytic expressions for the production and attenuation of neutrons and photons from electron beam loss at "thick targets" such as beam dumps or collimators. The five major electron radiation loss components considered are:

- Giant-Resonance-Neutrons (GRN): Those neutrons with energy range between 0.1 MeV and 20 MeV are photoproduced in the core of the shower.
- High-Energy-Neutrons (HEN): Neutrons with energy above 100 MeV are initiated by high energy photons in the hadronic cascade. The production angle is in the forward direction.
- Mid-Energy-Neutrons (MID): Neutrons having energies between GRN and HEN, being produced by quasi-deuteron reactions.
- Direct Gamma (GAMD): Photons leaving the core with energies between 0.1 MeV and 20 MeV.
- Indirect Gamma (GAMI): Photons and directly ionizing particles created during slowing down of the HEN.

8.3 Radiation protection boundary condition

According to the conceptual design, the area outside the accelerator bunker, though still inside the building, will be accessible for persons not occupationally exposed to ionizing radiation. In that sense the bunker shielding has to be dimensioned to keep the ambient dose equivalent rate below the limit of 0.125 µSv/h (the sum of both, the neutron- and γ-dose rate).

8.4 Shielding calculations

The operational conditions of the accelerator system to be built are as follows. The final 300 MeV electron beam will be generated by pulse operation with 10 Hz pulse frequency and 40 psec pulse width with a peak current of 5 A. The resulting charge per pulse is 200 pC and the total beam power is 0.6 watt. The beam will finally be dumped at the end of the beam line.

In Figure 40, the dose rate distribution for the five electron radiation loss contributions per beam loss of 1 watt, at a distance of 1 m from the iron target (length 30.5 cm, radius 5.1 cm) without any shielding are shown with respect to the beam forward direction. The dose rate maximum is located at a production angle ranging between 70 and 90 degrees. The major contribution found in the direction of 90 degrees (this defines the thickness of the lateral shielding) is mainly due to the direct photons from the electromagnetic shower with an energy range <20 MeV. The second main contribution is due to the Giant-Resonance neutrons, having energies between 0.1 MeV and 20 MeV.

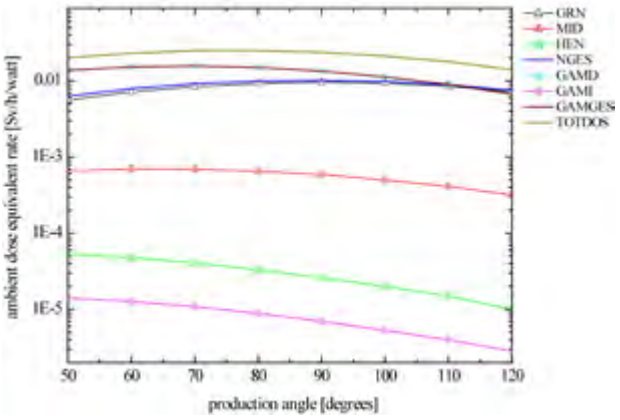

Figure 40: Dose rate distribution for the five main electron loss contributions, for a 1 watt beam-loss and a 0.3 MeV electron beam hitting the iron target, as a function of the production angle with respect to the beam forward direction, at distance of 1 m to the target. Abbreviations used: NGES = total neutron does rate, GAMGES = total γ-dose rate, TOTDOS = total dose rate

8.5 Lateral shielding

For the lateral shield calculation a shortest distance of 1.5 m between centre of beam and inner surface of the shielding is given according to the ground plan drawing of the injector building. The shielding wall is assumed to consist of normal concrete (ρ = 2.35 g/cm^3). Figure 42 shows the calculated shielding thickness distribution, as a function of a beam loss range between 0.025 and 0.1 watt, for the three chosen electron beam energies of 0.15 GeV (0.15 GeV is the threshold energy for the HEN production in SHIELD11), 0.2 GeV and 0.3 GeV respectively. The energy dependence of shielding thickness is small and ranges from 5 cm to less than 10 cm from the lowest to the highest beam losses considered.

An energy loss of about 5 % with respect to the total beam power may be assumed [60] which is 0.03 Watt, arising from some misalignment of the beam line. The shielding thickness required in order to be below the limits of the ambient dose rate, is between 114 cm and 118 cm, increasing with increasing beam loss. The missteered beam may strike structures such as collimators or iron yokes of the magnets, as well as some parts of the beam vacuum tube itself. As already mentioned, the SHIELD11 code is based on a “thick target” data approximation. In that sense, the thicknesses calculated for the lateral shielding certainly will express losses in collimators or other massive components. The inner surface of a beam pipe (thickness 3 mm) may be hit by an electron beam from grazing incidence (0.1 °C) to about 1 °C. The resulting effective thickness of the obstacle varies between 1.7 m and 17 cm, corresponding to about 100 and 10 radiation lengths in iron respectively. That is to say, an increasing deflection angle reduces target thickness in terms of radiation length. The neutron yield for iron for 1 GeV electrons increases by a factor of about 12 [61], when the target thickness varies from 2 up to 10 radiation lengths. It may be concluded that the lateral shielding thicknesses shown are conservative, considering interactions between electrons and the beam tube.

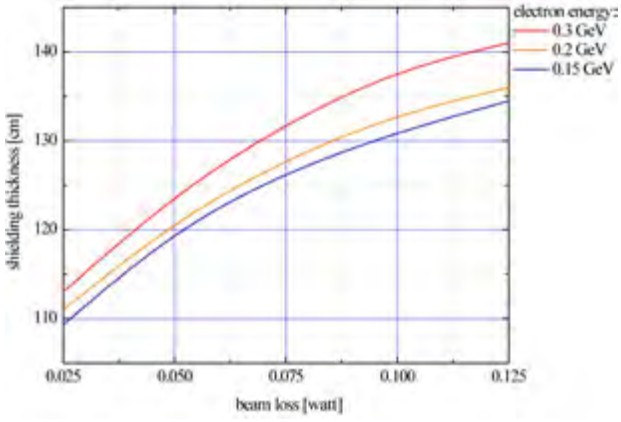

Figure 41: Concrete shielding thickness as a function of beam loss for several electron beam energies with the boundary condition of 0.125 μSv/h ambient dose equivalent rates outside the shielding wall (area of public access).

Nevertheless, considering the standard concrete-shielding-block thickness of 0.5 m and 1.0 m normally used at PSI, the results indicate demand for a special solution.

8.6 Shielding of the silo roof

In a first attempt, the situation on the silo bunker may be regarded as similar to the hall-floor. Allowing public access during beam operation leads to the same shielding thicknesses as for the lateral direction, presuming a distance of 1.5 m between the beam line and the inner surface of the concrete roof. If we consider the roof to be a controlled zone of type 0 for example, an ambient dose equivalent rate limit < 0 µSv/h would be tolerable for unrestricted access of occupationally exposed persons. In that case a roof thickness of 0.5 m would be sufficient to hold the limit for 0.03 watt beam loss at initial electron energy of 0.3 GeV. However the crane driver should also be treated as a person occupationally exposed to radiation (dosimeter wearing obligatory).

8.7 Shielding of the 0.3 GeV electron beam dump

The whole of the 0.6 watt 0.3 GeV electron beam will be dumped at the end of the test-beam line. The shielding calculations are based on a distance of 1.5 m between the downstream end of beam dump and the inner surface of the concrete wall and also laterally to the beam dump. The limit for the ambient equivalent dose rate outside the shielding is 0.125 µSv/h (area of public access). The beam dump core is expected to consist of steel. It can be shielded laterally and downstream with a layer of lead. In Table 20 several possible beam dump configurations are shown. Commonly the remaining γ-dose rate is about 2 % compared to the neutron generated one. A pure steel core target requires the longest dump and the thickest shielding wall respectively. Additional lead shielding in the forward direction allows for a reduction of the thickness of both, the steel core dump as well as the concrete shielding wall. The activation potential of the two metals is to be considered in the range of disposal.

The thickness of the lateral concrete shielding for the given beam dump lengths and geometries is affected only by the additional lateral lead shielding. In Table 21 the results for three different lead thicknesses are shown: 150 cm of concrete is adequate for a 15 cm lateral lead cladding applied to the steel core beam dump.

Length of beam dump iron (cm)	Addition lead downstream (cm)	Addition lead lateral (cm)	Thickness concrete wall downstream (cm)	γ-dose rate (μSv/h)	n-dose rate (μSv/h)	total-dose rate (μSv/h)
132	0	10	200	0.025	0.09	0.11
50	20	10	200	0.02	0.075	0.095
132	36	10	150	0.017	0.08	0.097
50	44	10	150	0.016	0.074	0.09

Table 20: Beam dump shielding in beam forward direction at production angle 0 degree.

Addition lead lateral [cm]	Resulting thick-ness of lateral concrete wall [cm]	γ-dose rate	Thickness concrete wall downstream (cm)	γ-dose rate (μSv/h)	n-dose rate (μSv/h)	total-dose rate (μSv/h)
10	153	0.013	0.081	0.094	0.09	0.11
12	150	0.013	0.081	0.094	0.075	0.095
15	145	0.012	0.083	0.095	0.08	0.097

Table 21: Lateral beam dump shielding at production angle 90 degree.

9 References

[1] Editor R. Ganter, SwissFEL CDR, to be published.

[2] C. Limborg *et al.,* "RF design of the LCLS gun",LCLS TN-05-03.

[3] T. Schietinger *et al.,* measuring and modeling at the PSI-XFEL 500-kV Low Emittance Electron Source, Proceedings of the LINAC 2008, Vancoover, Canada (2008).

[4] Y. Kim *et al.,* Beam Diagnostic and RF Systems Requirements for the SwisFEL Facility, Proceedings DIPAC09.

[5] B. E. Carlsten, Nucl. Instrum. Methods Phys. Res., Sect. A285, 313–319 (1989).

[6] C. Wang et al, Criteria for emittance compensation in high-brightness photoinjectors, PHYSICAL REVIEW SPECIAL TOPICS – ACCELERATORS AND BEAMS 10, 104201 (2007).

[7] Handbook of Accelerator Physics and Engineering, Sec. 2.4.4, p. 104, Eds. A. W. Chao, M. Tigner, World Schientific Publishing Co. Pte. Ltd., Singapore, ISBN 9810235005 / 91802388584 (2002).

[8] Recent Advances and Novel Ideas for High Brightness Electron Beam Production Based on Photo-Injectors M. Ferrario, M. Boscolo, V. Fusco, C. Vaccarezza, C. Ronsivalle, J. B. Rosenzweig, L. Serafini, LFN internal report SPARC-BD-03/003/LNF–03/06 (P), INFN, Frascati, Italy (2003).

[9] Envelope analysis of intense relativistic quasilaminar beams in rf photoinjectors: A theory of emittance compensation. L. Serafini, J. B. Rosenzweig, Phys. Rev. E., 55 (6), p. 7565 (1997).

[10] M. Altarelli et al, European Free-Electron Laser Technical Design Report (page 98).

[11] SLAC–R–593, Linac Coherent Light Source, Conceptual design report (paragraph 6.1).

[12] Y. Ding et al, SLAC-PUB-13525, January 2009.

[13] R. Ganter et al, Commissioning of a Diode/RF Photogun Combination, Proc. FEL 2009, Liverpool, UK.

[14] R. Bossard et all, CLIC note 297 and PS/RF note 95-25 (1995).

[15] R. Bossart, M. Dehler, DESIGN OF A RF GUN FOR HEAVY BEAM LOADING, EPAC 96 proceedings.

[16] L. Stingelin, FEL-SU84-001-Power_test-CTF-Gun, SwissFEL internal report.

[17] R. Losito et al, "The PHIN Photoinjector for the CTF3 drive beam", Proceeding EPAC 06.

[18] M. Dehler *et al.,* Phys. Rev.ST accelerators and beams 12, 2009.

[19] D. Alesini *et al.,* RF deflector design and measurements for the longitudinal and transverse phase space characterizationat SPARC, Nucl. Instrum. Meth. A 568, 488-502, 2006.

[20] G. D'Auria, private communications.

[21] L. Doolittle *et al.,* Digital Low-Level RF Control Using Non-IQ Sampling, Proceedings LINAC06, Knoxville, Tennessee USA.

[22] Y. Otake. Construction of XFEL/Spring8, Proceedings of FEL08, Gyeongju, Korea.

[23] S. Hunziker *et al.,* Toward an Ultra-Stable Reference Distribution for the Nex PSI 250 MeV Injector, proceeding DIPAC09, Basel Switzerland.

[24] A. Winter, private communication, 2007.

[25] E. Vogel, W. Koprek, P. Pucyk, in FPGA based RF field control at the photo cathode RF gun of the DESY vacuum ultraviolet free electron laser, Proceedings of the EPAC Conference, Edinburgh, Scotland, 2006.

[26] R. Akre, D. Dowell, P. Emma, J. Frisch, B. Hong, K. Kotturi, P. Krejcik, J. Wu, in LCLS LLRF Upgrades to the SLAC LINAC, Proceedings of the PAC Conference, Albuquerque, New Mexico, USA, 2007.

[27] C. Rivetta, R. Akre, K. Kotturi, in Operational Experience with LCLS RF systems, LCLS DOE Review, July 11, 2007.

[28] V. Schlott *et al.,* "Performance of the Digital BPM System for the Swiss Light Source", Proc. DIPAC'01, Grenoble, France, May 2001.

[29] M. Böge *et al.,* "User Operation and Upgrades of the Fast Orbit Feedback at the SLS", Proc. PAC'05, Knoxville, USA, May 2005.

[30] M. Dehler *et al.,* "State of the SLS Multi Bunch Feedbacks", Proc. APAC'07, Indore, India, Feb. 2007.

[31] A. Andersson *et al.,* "Recent Results from the Electron Beam Profile Monitor at the Swiss Light Source", Proc. DIPAC'07, Venice, Italy, May 2007.

[32] D. Sütterlin, "Single Shot Electron Bunch Length Measurements with a Spatial Electro-Optical Auto-Correlation Interferometer using Coherent Transition Radiation at the 100 MeV SLS Pre-Injector LINAC", PHD-thesis, Diss ETH Nr. 16668, ETH-Zürich 2006.

[33] V. Schlott *et al.,* "THz Diagnostic for the Femto Bunch Slicing Project at the Swiss Light Source", Proc. EPAC'06, Edinburgh, UK, June 2006.

[34] R. Ischebeck *et al.,* "Screen Monitor Design for the SwissFEL", Proc. DIPAC 2009, Basel, Switzerland, May 2009.

[35] A. Citterio *et al.,* "Design of a Resonant Stripline Beam Position Pickup for the 250 MeV PSI XFEL Test Injector", Proc. DIPAC 2009, Basel, Switzerland, May 2009.

[36] B. Keil *et al.,* " Application of a 5 GSPS Analogue Ring Sampling Chip for Low-cost Single-shot BPM Systems", Proc. EPAC 2008, Genoa, June 2008.

[37] See: http://www.bergoz.com/products/In-Flange.CT/In-Flange.CT.html

[38] B. Steffen *et al.,* "A Compact Single Shot Electro-Optical Bunch Length Monitor for the SwissFEL", DIPAC 2009, Basel, Switzerland, May 2009.

[39] F. Müller *et al.,* "Ytterbium Fiber Laser for Electro-Optical Pulse Length Measurements at the SwissFEL", DIPAC 2009, Basel, Switzerland, May 2009.

[40] F. Löhl *et al.,* "A Sub-50fs Bunch Arrival Time Monitor System for FLASH", Proc. DIPAC'07, Venice, Italy, May 2007.

[41] http://www.iapla.unibe.ch/

[42] B. J. Claessens *et al.,* Phys. Rev. Letters 95, 164801 (2005).

[43] www.fastlite.com

[44] B.W. Van Wonterghem et al, Proceedings of the Conference on Laser Coherence Control, SPIE 1870 (1993), p 64.

[45] www.quantel.fr

[46] C. Hauri et all, Intrinsic Emittance Reduction of an Electron Beam from Metal Photocathodes, Phys. Rev. Lett. 104, 234802 (2010).

[47] L. Canova et al, "Ultrashor tpulse generation with the Mazzler active spectral broadening and the XPW pulse shortening technique, Conference on Lasers an Electro-Optics, OSA Technical Digest 2008, paper JTuA39.

[48] LCLS Conceptual design report, *ssrl.slac.stanford.edu/lcls/cdr.*

[49] P. Wiegand, "SLS SR girder, vibration and modal analysis tests", SLS-TME-TA-2000-0153.

[50] Engineering Study Report on the Magnetic Elements and Girders for Swiss Light Source, BudkerInstitute, Novosibirsk, October 1997.

[51] Y. Kim *et al.,* Low Thermal Emittance Measurements at the SwissFEL Low Emittance Gun test Facility, Proceeding of FEL 08, Gyeongju, Korea.

[52] D. H. Dowell et al, Quantum efficiency and thermal emittance in metal photocathodes, Phys. Rev. Special Topics, Accelerator and beams, 12, 074201, 2009.

[53] Y. Kim *et al.,* Start to end simulations of the PSI 250 MeV injector test facility, proceedings of EPAC08, Genoa, Italy.

[54] L. Serafini, J. B. Rosenzweig, Phys. Rev. E 55.

[55] M. Ferrario *et al.,* SLAC-PUB-8400 (1997) 7565.

[56] J. Welch et al, LCLS compressor dipole field quality and beam measurements, Proceedings of FEL08, Gyeongju, Korea, 2008.

[57] www.vectorfields.com

[58] Memorandum "LEG Project New Building Shielding" Ch. Gough 29.05.06, PSI.

[59] The SHIELD11 Computer Code W. R. Nelson, T. M. Jenkins, SLAC-R-737, UC-414.

[60] Private communication Ch. Gough, PSI.

[61] "Giant dipole resonance neutron yields produced by electron as a function of target material and thickness", X. Mao *et al.,* SLAC-PUB-6628, 1996.

Published by
Paul Scherrer Institut

Coordination
Marco Pedrozzi

English Proofreading
Trevor Dury

Design and Layout
Irma Herzog

Photographs

Printing
Paul Scherrer Institut

Available from
Paul Scherrer Institut
Communications Services
5232 Villigen PSI, Switzerland
Phone +41 (0)56 310 21 11
www.psi.ch

PSI public relations
pubrel@psi.ch

Paul Scherrer Institut
July 2010

Paul Scherrer Institut, 5232 Villigen PSI, Switzerland
Tel. +41 (0)56 310 21 11, Fax +41 (0)56 310 21 99
www.psi.ch